AD-A191 558 OPTICAL NONLINEARITIES IN GAAS/GAALAS MULTIPLE QUANTUM WELLS FABRICATED B (U) UNIVERSITY OF SOUTHERN CALIFORNIA LOS ANGELES DEPT OF ELECTRI 1/1

UNCLASSIFIED E GAMIRE ET AL DEC 87 AFOSR-TR-88-0130 F/G 20/12 NL

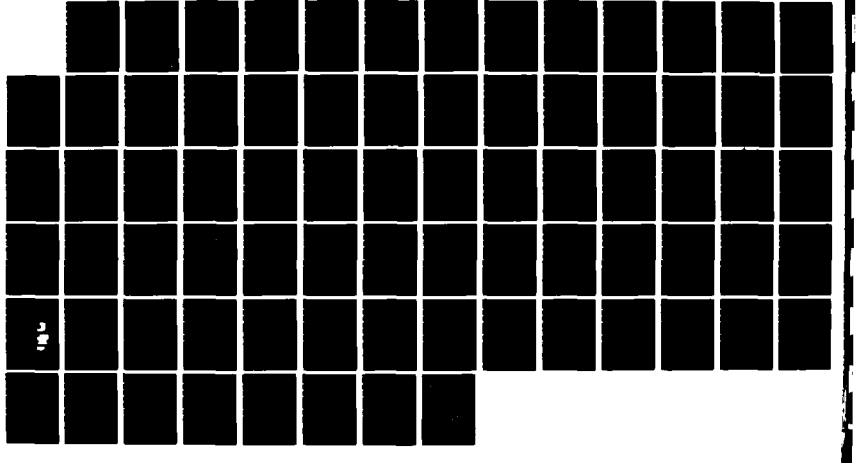

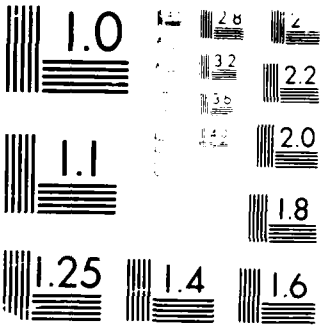

DTIC FILE COPY

2

AD-A191 558

UMENTATION PAGE

Form Approved
OMB No. 0704-0188

1b. RESTRICTIVE MARKINGS

2a. SECURITY CLASSIFICATION AUTHORITY

3. DISTRIBUTION/AVAILABILITY OF REPORT
Approved for public release, distribution unlimited

2b. DECLASSIFICATION/DOWNGRADING SCHEDULE

4. PERFORMING ORGANIZATION REPORT NUMBER(S)

5. MONITORING ORGANIZATION REPORT NUMBER(S)
AFOSR-TR- 88-0130

6a. NAME OF PERFORMING ORGANIZATION	6b. OFFICE SYMBOL (If applicable)	7a. NAME OF MONITORING ORGANIZATION
Univ of California		AFOSR/Ne

6c. ADDRESS (City, State, and ZIP Code)	7b. ADDRESS (City, State, and ZIP Code)
Los Angeles, CA 90089-0483	Bldg 410
Bolling	AFB, Bolling AFB, DC 20332-6448

8a. NAME OF FUNDING/SPONSORING ORGANIZATION	8b. OFFICE SYMBOL (If applicable)	9. PROCUREMENT INSTRUMENT IDENTIFICATION NUMBER
AFOSR	NE	AFOSR-85-0297

8c. ADDRESS (City, State, and ZIP Code)	10. SOURCE OF FUNDING NUMBERS			
	PROGRAM ELEMENT NO	PROJECT NO	TASK NO	WORK UNIT ACCESSION NO
Bldg 410 Bolling AFB, DC 20332-6448	61102F	2305/	B1	

11. TITLE (Include Security Classification)
OPTICAL NONLINEARITIES IN GaAs/GaAlAs Multiple Quantum WELLS FABRICATED BY METALORGANIC CHEMICAL VAPOR DEPOSITION FOR USE IN OPTICAL SIGNAL PROCESSING

12. PERSONAL AUTHOR(S)
GARMIRE

13a. TYPE OF REPORT	13b. TIME COVERED	14. DATE OF REPORT (Year, Month, Day)	15. PAGE COUNT
Final	FROM 01/08/85 TO 01/06/87		

16. SUPPLEMENTARY NOTATION

17. COSATI CODES			18. SUBJECT TERMS (Continue on reverse if necessary and identify by block number)
FIELD	GROUP	SUB-GROUP	

19. ABSTRACT (Continue on reverse if necessary and identify by block number)

Preparation of high quality GaAs/GaAlAs Multiple quantum wells (MQW) grown by Metalorganic Chemical Vapor Deposition on GaAs substrates and measurement of nonlinear saturation has been completed in this 18 month contract. The results show materials which rivals the highest quality MQW's grown by any technique. Preparation of GaAs/GaAlAs MQW's on GaP substrates and measurement of nonlinear saturation has been completed. It was shown that this material has high cw saturation intensity and, if used in a nonlinear Fabry-Perot, would be useful only in pulsed experiments. The material looks ideal for hybrid devices.

DTIC ELECTE FEB 29 1988 S E

20. DISTRIBUTION/AVAILABILITY OF ABSTRACT	21. ABSTRACT SECURITY CLASSIFICATION
☐ UNCLASSIFIED/UNLIMITED ☐ SAME AS RPT ☐ DTIC USERS	UNCLASSIFIED

22a. NAME OF RESPONSIBLE INDIVIDUAL	22b. TELEPHONE (Include Area Code)	22c. OFFICE SYMBOL
GILES	202 767-4933	NE

DD Form 1473, JUN 86 — Previous editions are obsolete — SECURITY CLASSIFICATION OF THIS PAGE

AFOSR-TR- 88-0130

Final Report

Optical Nonlinearities in GaAs/GaAlAs Multiple Quantum Wells fabricated by Metalorganic Chemical Vapor Deposition for use in Optical Signal Processing

Submitted to
Dr. Lee Giles
AFOSR
Bolling Air Force Base
Washington, D. C.

by

E. Garmire and P. D. Dapkus
Department of Electrical Engineering
University of Southern California
Los Angeles, CA 90089-0483

December, 1987

Abstract

Preparation of high quality GaAs/GaAlAs Multiple quantum wells (MQW) grown by Metalorganic Chemical Vapor Deposition on GaAs substrates and measurement of nonlinear saturation has been completed in this 18-month contract. The results show material which rivals the highest quality MQW's grown by any technique. Preparation of GaAs/GaAlAs MQW"s on GaP substrates and measurement of nonlinear saturation has also been completed. It was shown that this material has high cw saturation intensity and, if used in a nonlinear Fabry-Perot, would be useful only in pulsed experiments. The material looks ideal for hybrid devices, however.

Modelling of the nonlinear Fabry-Perot based on the experimental determination of the saturable absorption and the corresponding nonlinear refractive index has shown that operation on reflection, very near the exciton resonance, will give low threshold bistability (<1mW/pixel) with very high on-off ratios suitable for optical computing applications.

GaAs/GaAlAs Mutiple Quantum Wells Fabricated by Metalorganic Chemical Vapor Deposition for use in Optical Signal Processing

Introduction

The research carried out on this contract had three main goals, all of which were met. The first was to prepare high quality mutiple quantum wells (MQW) by metalorganic chemical vapor deposition (MOCVD) and to measure the nonlinear refractive index in these materials. This was done by measuring the saturation in the absorption and using Kramers Kronig relationships to determine the nonlinear refractive index.

The second goal was to fabricate and test MQW's grown on transparent substrates, chosen to be GaP. The result of this effort was single crystal material with carrier lifetimes short enough that the saturation intensity was higher than for MQW's fabricated on GaAs. Projections for the use of this material are in hybrid devices.

The third goal was to fabricate distributed Bragg reflector (DBR) layers on a substrate prior to the growth of MQW's. Such reflectors can provide nonlinear Fabry-Perots and (NLFP) and devices which may be used in reflection without removing the substrate. High reflectance multi-layers were successfully grown by MOCVD.

This report is divided in the following sections: Section II contains the paper which was published in Applied Physics Letters, describing the first measurements of nonlinear effects in MOCVD-grown materials. These results demonstrate the lowest saturation intensities reported by any technique. Further documentation of various portions of the work are found in the theses of H. C. Lee (PhD) and M. Kawase (MS).

Section III contains an invited paper submittted to Journal of Quantum Electronics discussing our experimental results and analysis of the structure dependence of MQW nonlinear optical properties.

Section IV shows recent results obtained in MQW structures on GaP substrates. In these we demonstrate the electroabsorption properties of these structures. Also discussed is our data on the growth of high reflectivity DBR reflectors.

Section V contains discussions of our work relevant to optical computing applications. In particular, we make projections about the use of NLFP devices in parallel digital systems.

II. The first demonstration of nonlinear absorption in MOCVD grown materials.

The following paper describes our initial investigations into the controlling growth parameters for achieving strong excitonic resonances and and low threshold nonlinear absorption. It was published in Applied Physics Letters **50**,1182 (1987).

Nonlinear absorption in AlGaAs/GaAs multiple quantum well structures grown by metalorganic chemical vapor deposition

H. C. Lee, A. Hariz, and P. D. Dapkus
Center for Photonic Technology, Department of Electrical Engineering, University of Southern California, Los Angeles, California 90089-0483

A. Kost, M. Kawase, and E. Garmire
Center for Laser Studies, Department of Electrical Engineering, University of Southern California, Los Angeles, California 90089-0483

Received 8 December 1986; accepted for publication 27 February 1987.

We report the study of growth conditions for achieving the sharp exciton resonances and low intensity saturation of these resonances in AlGaAs-GaAs multiple quantum well structures grown by metalorganic chemical vapor deposition. Low growth temperature is necessary to observe this sharp resonance feature at room temperature. The optimal growth conditions are a tradeoff between the high temperatures required for high quality AlGaAs and low temperatures required for high-purity GaAs. A strong optical saturation of the excitonic absorption has been observed. A saturation density as low as 25 W/cm^2 is reported.

There has been a great deal of interest in developing low-loss, high-speed nonlinear optical switching and signal processing elements for future optical computing and information processing systems. The criteria for these elements to be practical are that they possess large optical nonlinearities at room temperature with low saturation intensities, and a fast response time. AlGaAs-GaAs multiple quantum wells (MQW's) are promising for these applications and have drawn a great deal of attention in recent years. The room temperature nonlinear optical properties of excitons in these structures have been studied intensely.[1–3] A strong excitonic absorption resonance can be seen in MQW structures at room temperature because of the quantum size effect, which increases the binding energy of the correlated electron-hole pairs.[4] Nonlinear absorption can be accomplished by bleaching the exciton resonance with free carriers.

The most widely used techniques for growing such ultrathin, abrupt multilayers are molecular beam epitaxy (MBE) and metalorganic chemical vapor deposition (MOCVD). Efficient, narrow-linewidth luminescence and low-threshold laser operation have been achieved in MQW's grown by both techniques.[5,6] However, even though exciton resonances have been seen in MQW's grown by MOCVD in linear absorption spectra,[7] virtually all of the reported work dealing with nonlinear optical properties to date have employed MBE-grown materials.[1–3] The implementation of arrays of optical bistable switches in optical computing and processing systems requires large area devices with high uniformities. It is the potential advantages of MOCVD for large area, high throughput, multiple wafer growth of these complex structures that provides the motivation to explore this technique. In this letter, we study the growth conditions for achieving room-temperature excitonic absorption in AlGaAs-GaAs MQW structures grown by MOCVD. It is found that, as with temperature to achieve high AlGaAs quality, low impurity concentration and high luminescence efficiency are required for GaAs. The linear and nonlinear optical properties of these structures are described. Room-temperature exciton nonlinear absorption with low saturation intensity is also reported.

Enhanced exciton absorption in MQW structures requires low concentrations of free carriers and controlled impurities to avoid ionizing the exciton and Stark broadening of the exciton linewidth. Additionally, low threshold nonlinear effects, which are desirable for low operating energy, require long minority-carrier lifetimes and high internal quantum efficiency in the quantum wells. These conditions present a set of conflicting requirements upon the MOCVD growth parameters. The purity of GaAs grown by MOCVD increases rapidly with decreasing growth temperature. The highest purity materials grown by MOCVD are in the range of 600–650 °C.[8] On the other hand, even though the background impurity concentration in AlGaAs is observed to increase at high growth temperatures, higher luminescence efficiencies and longer minority-carrier lifetimes in bulk AlGaAs materials and MQW structures are observed in samples grown at relatively high temperatures, 750–800 °C.[9] Deep levels, which are believed to be caused by an Al-O complex,[9] form at low growth temperatures and degrade the quantum efficiency. The tradeoffs for achieving strong excitonic absorption in room-temperature MQW's by MOCVD have been determined in this study and will be examined in the discussion.

The structural properties of the samples studied are summarized in Table I. All samples were grown by atmospheric pressure MOCVD. Trimethylgallium and triethylaluminum were used for Ga and Al sources, respectively. Arsine gas was purified by an in-line molecular sieve. The reactor is designed to minimize the interfacial transition width in the MQW's. It employs differential pressure transducers in a vent run configuration to dynamically balance the pressures and flow rates during alternate source gas retention times. Figure 1 shows the photoluminescence (PL) spectra of three representative MQW structures grown at different temperatures. The spectra contain two peaks

TABLE I. Characteristics of GaAs/AlGaAs samples.

Sample	N	TMGa flow rate (sccm)	Growth temperature (°C)	Barrier Al composition	Number of periods	Well thickness (Å)	Barrier thickness (Å)	ΔE_c (eV)	ΔE_v (eV)	L_z (Å)	LWHM (Å)
v158	1	TMG	650	0.3	50	200	200	0.2	0.137	140	5.6
v159	1	TMG	700	0.3	50	200	200	0.2	0.137	140	5.6
v160	1	TMG	750	0.3	50	200	200	0.2	0.137	140	5.6
v136	1	AVA	750	0.3	50	200	200	0.2	0.137	140	5.6

caused by transitions from the $n = 1$ electron state to the $n = 1$ light- and heavy-hole states, respectively. Figure 2 shows the dependence of the relative PL intensity upon excitation intensity for two samples. Sample v158, grown at lower temperature (650 °C), has narrower PL linewidth and lower PL efficiency than those grown at higher temperatures. The low efficiency of sample v158 originates from the low free carrier concentration in the GaAs wells and the higher trap densities in AlGaAs barriers as the result of low growth temperature. Note that in Fig. 2 the traps of sample v158 can be filled at relatively small intensities, resulting in a saturation effect in the PL intensity versus excitation intensity curve. It is noted that in the samples grown at higher temperatures PL linewidth, both in the GaAs and AlGaAs layers, increases steadily with increasing growth temperature. This trend is similar to that observed in MBE grown samples. We believe that the main reason for the increased linewidth in our samples is the increase with the growth temperature of the impurity concentration in the structure with the growth temperature. The samples of this study have wells thick enough that the PL linewidths are insensitive to interface roughness and lateral terrace dimensions.[16] In fact, thinner quantum wells do not show the strong dependence of PL linewidth upon growth temperature observed by other workers.[17] The interface formation is likely to be a kinetic phenomenon and, as a result, will be reactor dependent.

For absorption measurements, the substrates of MQW samples were removed by selective etching using a mixture of NH_4OH and H_2O_2 with pH value in the range of 9–10.[18] Measurements of PL were performed subsequently on the bare grown layers to confirm that the linewidths were uniform throughout the structures. Figure 3 shows room-temperature linear absorption measurements for samples grown at different temperatures. Enhanced absorption near the band edge, ascribed to the exciton resonance, is observed in samples with low carrier concentration. The sample with the highest carrier concentration (v136) was grown with a less pure source of trimethylgallium and shows no resolved exciton absorption feature at all. Higher resolution evidence for the presence of excitonic absorption has been observed in room-temperature excitation spectra of sample v158.[19] The heavy- and light-hole exciton transitions are well resolved in this case and agree with the PL data.

Absorption saturation has been observed in sample v158 both on and off the exciton resonance. The cw excitation was provided by an argon-ion laser-pumped dye laser. Styryl-9M

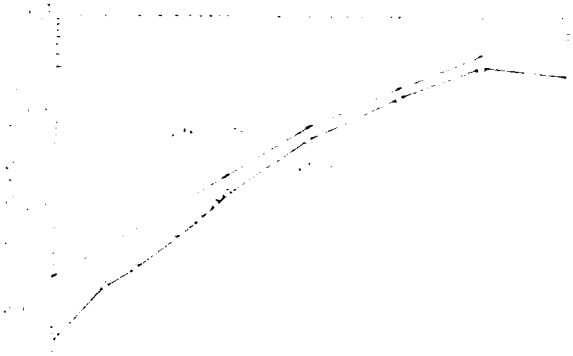

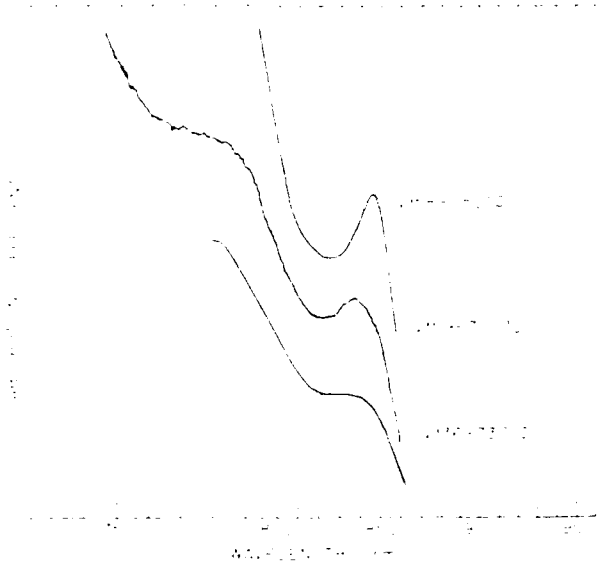

FIG. 3. Absorption spectra of MQW structures grown at 650, 700, and 750 °C.

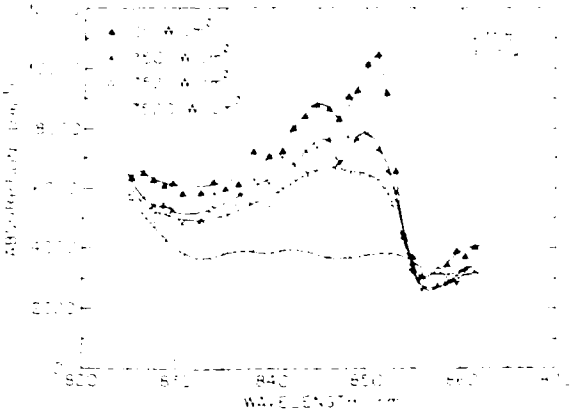

FIG. 4. Absorption vs wavelength at different excitation intensities: ▲ 25 W/cm², ○ 251 W/cm², □ 752 W/cm², ◇ 7520 W/cm².

dye was used to provide wavelengths in the range 780–900 nm. Sufficient dynamic range for the excitation intensity was obtained by using an acousto-optic modulator to vary the power of incident beam. Both incident and transmitted beams were monitored at the same time. The beam size was measured to be 14 μm × 17 μm. Bulk sample heating was avoided by modulating the incident beam with a low duty cycle chopper. Filamentary heating was estimated to be negligible for the intensities we used. In Fig. 4 the bleaching of excitonic absorption is clearly seen in the absorption spectra under various excitations. The two sharp and well-resolved absorption peaks observed under low excitation intensities were attributed to excitons associated with heavy holes and light holes, respectively. These are consistent with the excitation spectrum. The distinct excitonic absorption enhancement is saturated at low intensities and merges with the background absorption as shown in Fig. 4. Further saturation is caused by the effect of band filling and requires much higher excitation intensities. The highest intensity data have been corrected to account for Fabry–Perot effects. The saturation intensity of excitonic absorption determined from the data of Fig. 4 and from a measurement of the intensity dependence of the resonance absorption coefficient is 250 W/cm².

In conclusion, low-temperature MOCVD growth is necessary to achieve low free-carrier concentration and well-resolved excitonic absorption at room temperature. Even though such low growth temperatures result defects in the AlGaAs barriers and cause a degraded luminescence efficiency, these defects appear to play less role in the absorption properties of quantum wells and they may well be saturated at intensities below that required to saturate the exciton resonance. It should be noted that the purity of the trimethylgallium source material also has an impact on the purity of the MQW samples and the presence of excitonic features. Thus, source purity will affect the growth temperature at which exciton resonances can be observed. Finally, nonlinear absorption with low saturation intensity has been observed in MQW's grown by MOCVD. A saturation intensity of 250 W/cm² has been measured in optimized materials. This is comparable to the best reported values.[12]

The authors would like to thank Dr. W. H. Steier and Dr. J. Kumar for technical discussions and N. Watanabe and Y. Mori for access to unpublished work. This work has been partially supported by Air Force Office of Science Research grants 84-305 and 85-0297, NASA grant NAG 3-529, University of Southern California's Joint Services Electronics Program, the Army Research Office, and the National Science Foundation.

[1] D. S. Chemla, D. A. B. Miller, and P. W. Smith, Opt. Eng. **24**, 556 (1985).
[2] D. S. Chemla, J. Lumin. **30**, 502 (1985).
[3] D. S. Chemla, D. A. B. Miller, P. W. Smith, A. C. Gossard, W. Wiegmann, IEEE J. Quantum Electron. **20**, 265 (1984).
[4] D. S. Chemla and D. A. B. Miller, J. Opt. Soc. Am. B **2**, 1155 (1985).
[5] S. W. Koch, N. Peyghambarian, K. Hess, D. A. Gulotty, H. G. Drickamer, J. J. Coleman, and P. D. Dapkus, Appl. Phys. Lett. **40**, 922 (1982).
[6] P. D. Dapkus, H. M. Manasevit, K. L. Hess, T. S. Low, and G. E. Stillman, J. Cryst. Growth **55**, 10 (1981).
[7] E. F. Wagner and G. B. Stringfellow, J. Electron. Mater. **10**, 239 (1981).
[8] R. C. Miller, D. D. Dapkus, and P. M. Petroff, Appl. Phys. Lett. **44**, 808 (1984).
[9] P. K. Bhattacharya, R. Mallavarpu, and S. Subramanian, J. Cryst. Growth **68**, 536 (1984).
[10] J. Singh and K. K. Bajaj, Appl. Phys. Lett. **44**, 1075 (1984).
[11] N. Watanabe and Y. Mori, J. Cryst. Growth, to be published.
[12] D. A. B. Miller, D. S. Chemla, D. J. Eilenberger, P. W. Smith, A. C. Gossard, and W. T. Tsang, Appl. Phys. Lett. **41**, 679 (1982).

III. The structure dependence of the nonlinearities in AlGaAs/GaAs MQW's.

The following paper has been submitted as an invited contribution to the 1988 Special Issue on the Physics of Quantum Wells. The paper describes measurements of absorption saturation for various well widths and coupled with minority carrier lifetime measurements allows one to determine the fundamental properties of quantum wells that control the saturation intensity.

The Nonlinear Absorption Properties of AlGaAs/GaAs Multiple Quantum Wells Grown by Metalorganic Chemical Vapor Deposition

H. C. Lee[†], A. Kost[*], M. Kawase[*], A. Hariz[†], P. D. Dapkus[†] and E. Garmire[*]
Department of Electrical Engineering
[†]Center for Photonic Technology
[*]Center for Laser Studies
University of Southern California
Los Angeles, CA 90089

Abstract

The nonlinear absorption properties of the excitonic resonances associated with multiple quantum wells in AlGaAs/GaAs grown by metalorganic chemical vapor deposition are reported. The dependence of the saturation properties on growth parameters, especially growth temperature, and the well width are described. It is found that the minimum measured saturation intensity for these materials is of the order 250 W/cm^2. When corrected for lateral diffusion effects and the measured minority carrier lifetime, the data suggest that saturation intensities as low as 2.3 W/cm^2 can be achieved in this system. The growth of MQW structures on transparent GaP substrates is demonstrated and the electroabsorption properties of these structures are reviewed.

I. Introduction

Multiple quantum wells (MQW) have become an important class of materials for optoelectronic devices. In particular, a great deal of work has been devoted to exploring their use as nonlinear optical materials in bistable optical devices, nonlinear waveguide switches and optoelectronic electroabsorption switches. The purpose of the work reported in this paper is to explore the limits to the utilization of MQW's in these applications by determining the dependence of the nonlinear optical absorption on the materials properties and the structural design of the quantum wells. In addition, potential solutions to a fundamental technological issue in AlGaAs/GaAs MQW structures - the opacity of the substrate to near band edge radiation - are explored and presented.

The quantum confinement of electrons and holes in quantum wells gives rise to an absorption spectrum that is fundamentally different from bulk materials [1]. First, the energy distributions of the conduction and valence band states are altered to a step-like distribution characteristic of a quasi-two-dimensional solid. The positions of these density steps are associated with the allowed energies of the "square well potential" and are a strong function of the dimensions of the well and the composition of the barrier. In addition, the confinement increases the oscillator strength and the binding energy of free excitons in these layers resulting in strong excitonic resonances at each of the steps in the linear absorption spectra of these materials [2]. These resonances can be saturated by optical excitation [3]; an effect that has been used to fabricate nonlinear waveguide elements [4] and two dimensional bistable switching arrays [5]. The resonances have also been observed to persist in presence of large electric fields applied perpendicular to the layers [6] and to broaden and shift to lower energies with increasing field strength. This effect has been called the quantum confined Stark effect (QCSE) [6]. The QCSE has been exploited by Miller and co-workers [7] to develop optoelectronic switches such as the self-enhanced electroptic device (SEED). Application of the switching devices has been limited by the excessive power requirements of the nonlinear optical devices [8] and the complex processing required for the optoelectronc switches. In this paper we will address the minimum optical power required for the saturation of the absorption in quantum wells based on direct measurement of the controlling properties. We will also demonstrate a new

technology for the growth of quantum wells on transparent substrates that may mediate the fabrication difficulties inherent in optoelectronic switches.

The AlGaAs/GaAs MQW materials used in the studies presented here have been grown by metalorganic chemical vapor deposition (MOCVD) [9]. The materials properties and their dependence on the growth parameters will hopefully provide guidelines for the application of this technolgy to the fabrication of MQW nonlinear optical devices. The paper is organized so that the experimental methods of crystal growth and characterization are described first (Section II). The linear optical and optoelectronic properties of the materials structures are then presented followed by the nonlinear optical characteristics (Sections III, IV, and V). Section VI presents analysis of these properties that allows the extraction of the fundamental factors controlling the nonlinear properties of these materials. Section VII describes alternate structures for nonlinear and optoelectronic switch arrays and Section VIII summarizes the results and implications of these studies.

II. Experimental Techniques

A. Crystal Growth

All samples were grown by atmospheric pressure MOCVD [10,11]. The reactor is designed to minimize the interfacial transition width in the MQW's [12]. It employs differential pressure transducers in a vent/run configuration to dynamically balance the pressure and high flow rates (9 slpm) to reduce the gas retention time. Trimethylgallium and trimethylaluminum were used for Ga and Al sources respectively. Arsine gas was purified by an in-line molecular sieve. The operation of the manifold switching and critical flow rates are computer controlled. All MQW layers discussed in this paper were nominally undoped. The samples grown for this study were grown in the temperature range 650°C to 750°C. The background carrier concentration in undoped GaAs is observed to vary with source quality and growth temperature. This parameter will be discussed later.

The typical sample employed for the studies reported is as shown in Fig.1. It consists of 1.0 - 2.0 μm of MQW material surrounded by thicker confinement layers of $Al_{0.32}Ga_{0.68}As$. The growth is initiated by the growth of a thin

(100)GaAs GaAs layer followed by a 0.5 μm AlGaAs layer with high Al composition to act as an etch stop layer for substrate removal. The substrate was n-type (100) oriented horizontal Bridgeman - grown GaAs. The MQW material consisted of enough periods of the alternating structure to yield 0.39 - 0.54 μm of GaAs quantum wells. The spacer layers were 100Å in thickeness for all but the 50Å wells. In this case the barrier thickness was 150Å to minimize wave function overlap due to tunneling between the wells. The barrier layers were $Al_{0.32}Ga_{0.68}As$. The top and bottom confinement layers of structures used for electroabsorption modulators were doped p-type with diethylzine and n-type with disilane, respectively. Samples grown on transparent GaP substrates utilized a 2.0-3.0 μm thick $GaAs_{0.6}P_{0.4}$ intermediate buffer layer to reduce strain and dislocation density in the transition between the substrate and the MQW layers [13]. The GaP substrates used were (100) oriented and Czochralski-grown.

B. Optical Sample Preparation

Samples were typically used as-grown for CW and transient photoluminescence studies. Linear and nonlinear absorption measurements were performed after antireflection coating of the top surface and removal of the substrate using mechanical polishing, calibrated bulk etching and a selective GaAs etch [14]. The samples were mounted on glass in a strain free manner with transparent adhesives. An antireflection coating was applied to the back surface. A single surface reflectivity of 0.08 was measured on these samples.

C. CW and Transient Photoluminescence Characterization

The photoluminescence (PL) characteristics of the quantum well samples were measured at room temperature under low level CW conditions by exciting the samples with the 5145 Å line of an argon ion laser. The power density was kept low enough (~10 mW/cm^2) to avoid heating. The light was dispersed by a one meter monochromator and detected using phase sensitive techniques with an S-1 photomultiplier.

The transient PL measurements were performed by exciting the sample with the output of a pulsed commercial AlGaAs/GaAs QW laser array. A pulser with a 1 nsec fall time was used to achieve a light pulse with a fall time of 2-3

nsec. The wavelength of the laser was 7800Å and its output power was variable up to 1W peak. The light from the sample was dispersed by a one meter monochronomator and was detected using photon counting techniques with a GaAs photocathode photomultiplier. The transient response of the luminescence was measured by the delayed coincidence technique [15]. The total system response time was limited by the laser fall time.

D. Linear and Nonlinear Absorption Measurements

The low level absorption properties of the MQW samples were measured in transmission with a commercial UV-VIS spectrometer or with the attenuated output of a CW dye laser. In the latter case care was taken to insure that the excitation level was low enough to avoid the nonlinear absorption regime.

The nonlinear absorption properties of the MQW materials were measured by using an argon ion laser-pumped styrl-9 CW dye laser. The output power of the laser was attenuated by the use of an acousto-optic modulator. The first order diffracted beam was selected with an aperature. This system provided a 2000:1 dynamic range. The modulator output was pulsed with a 2 μsec duration for high level excitation or a 200 μsec duration for low level excitation. The repetition period was chosen to be 10 msec. The incident, reflected and transmitted beams were measured with calibrated photodiodes through the use of a beam splitter assembly and suitable neutral density filters. The spot was focussed to an area of a few hundred square microns by a long working distance lens assembly.

III. Linear Optical Properties

Early studies indicated that the major growth parameter controlling the nonlinear optical properties of MQW's grown by MOCVD was growth temperature [16]. The dependence of the nonlinear absorption properties on the quantum well width is also of importance as a fundamental issue. In addition, this variation may depend upon the growth process and was, in any case, unknown. As a result, a study to measure the variation of relevant properties as a function of both parameters was undertaken. In Fig.2 we show the dependence on growth temperature of the room temperature PL of three

samples with 100Å quantum wells grown at various temperatures ranging from 650°C to 750°C. The structural and electrical characteristics of these samples are listed in Table 1. The key points to be made are that the PL spectra of all samples shows the presence of the lowest energy (n=1) confined state transitions terminating in the heavy hole (hh) and light hole (lh) valence band states and that the width of the spectra increases slightly with increasing growth temperature. The increasing spectral width reflects, we believe, the increased concentration of free carriers in the well owing to an increase in the background carrier concentration with increased growth temperature. This trend is consistent with the electrical properties of bulk GaAs samples grown under same conditions as shown in Table I [17]. This is further supported by the fact that the linewidth of the high purity samples increases by several meV at higher excitation levels and thus higher carrier concentrations.

The absorption properties of samples grown at various temperature also show the effect of increasing impurity concentration at higher growth temperatures as shown in the low resolution spectra of Fig. 3. The sample grown at 650°C exhibits a well defined excitonic resonance characteristic of MQW's while the resonance for the sample grown at 700°C is somewhat broadened and reduced in amplitude. The third sample shown was grown at 750°C with an impure Ga source. It has relatively high background carrier concentration and exhibits no excitonic absorption resonance.

The PL properties of samples grown at 700°C with various quantum well widths are shown in Fig 4. The properties of the samples are shown in Table 2. The wells range from 54Å to 193Å in width as judged by the peak position of the n=1, hh PL transition and the energy differences between the other transitions. In the narrow wells, the light and heavy hole transitions are well resolved owing to the larger energy separation of the terminal states. The spectra of the thicker wells show peaks due to transitions from the n=2 and n=3 electron states. The occupation of these states is made possible by the decreased separation from the n=1 state as the well width is increased.

The room temperature linear absorption spectra of the same samples is shown in Fig.5. Note the step-like nature of the absorption and the presence of resonances associated with the n=1 transitions. Both of these features are

unique to these quasi two dimensional systems. Note that the spectral width of the transmission spectra is comparable to the PL spectral width in these samples. Because the PL laser excitation hardly penetrates the top cladding layer we expect that only the first few wells are excited by the carriers that diffuse from the cladding layer. The close correspondence between the emission and absorption linewidths suggests that the well width is extremely uniform from well to well through the samples.

IV. Minority Carrier Lifetime

The minority carrier lifetime of quantum well samples was measured by monitoring the PL decay time under the pulsed excitation. For optical transitions involving free carriers or weakly bound excitations such as free excitons, the PL decay time accurately reflects the minority carrier lifetime. We have chosen to use photon energies in the excitation that are directly absorbed by the quantum well layers to avoid possible ambiguities involving nonunifrom excitation or carrier capture by the wells. The PL time decays of three previously discussed samples grown at various temperatures are shown in Fig. 6. The measurements were performed at the highest excitation intensity allowed by experimental conditions (≈ 50 W/cm^2) to simulate as close as possible the high level conditions involved in absorption saturation. This limit was set by the power of the laser and the need to maintain a spot size large enough to avoid any lateral diffusion effects on the measurement. The time decay of each of the samples contains a dominant component that is exponential over 2-3 orders of magnitude. This component of the decay time also increases with increasing growth temperature. This is consistent with the trend observed in the PL efficiency. The samples grown at the higher temperatures exhibit an initial decay that is somewhat shorter than the dominant decay mode and a transition to a shorter decay at longer times. The latter effect is the result of emptying of saturated recombination centers in the material at longer times, which increases the rate of minority carrier recombination. We have studied these effects in detail and will report them in a separate publication. We have observed, however, that samples with longer minority carrier lifetimes at low levels exhibit strong increases in the lifetime with excitation, presumably because there are fewer recombination centers in the material and they are more easily saturated as a result. The shorter initial

decay component in the samples with long minority carrier lifetimes is the result of the short pulse excitation used in these experiments . It may be regarded as the time for the carriers to establish steady state conditions.

Table 3 lists the PL decay times of the absorption samples with different well widths. The decay time is observed to decrease with decreasing well width. The longest decay times we have observed exceed 1 μsec. This, we believe, is a reflection of the high quality of our samples. The dependence of lifetime on the well width reflects increased penetration of the electron and hole wave function into the lower quality barrier layers where the nonradiative recombination rate is higher. This observation is consistent with the data of Fig. 6 because the dominant effect of growth temperature on the PL efficiency is to improve the quality of the AlGaAs barrier layers.

V. Nonlinear Absorption Properties

Saturation Intensity

The transmission spectra of all samples exhibit Fabry-Perot resonance peaks due to the residual reflectivity of the front and back surfaces. In Fig 7 a we show the transmission spectra of the sample with the 72Å well width. The low intensity spectrum shows transmission minima at 829 nm and 837 nm that correspond to the n=1 light and heavy hole absorption resonances. The local minima at 822 nm and 855 nm correspond to destructive interference of the reflections from the front and back surfaces. In all cases the wavelength separation of these resonances agreed with the expected separation based upon the known thickness of the samples. These minima must be treated to accurately determine the absorption coefficient. The Fabry - Perot resonances were removed from the spectra by analyzing the spectra according to the following relationship:

$$T = \frac{(1-R_f)(1-R_b)\,e^{-\alpha L}}{(1-R_{eff})^2} \cdot \frac{1}{1+F\sin^2(\delta/2)} \qquad (1)$$

where R_f and R_b are the front and back surface reflectivities, respectively, α is the absorption coefficient, L is the integrated quantum well thickness,

$R_{eff} = e^{-aL} (R_f R_b)^{1/2}$ is the effective mean reflectance, $F = 4 R_{eff} / (1-R_{eff})^2$ is the finesse and δ is the wavelength dependent phase that depends on the optical length in the cavity. The absorption coefficient can be determined from (1) and the experimental data . We used $R_f = 0.08$ and $R_b = 0.1$. $\delta(\lambda)$ was determined from the resonances in the spectra at high excitation. Fig.7b shows the absorption spectra of this sample at several intensities. Note that the Fabry - Perot effects have been completely removed from the spectra.

The light and heavy hole excitonic resonances in the absorption spectra of Fig. 7 are saturable at moderate intensities. In Fig. 8a we show the excitation dependence of the absorption coefficient of sample V158. Note that the heavy hole exciton resonance decreases in amplitude at a rather modest input intensity. It also decreases more rapidly with excitation than the light hole resonance or the continuum. We have reported a saturation intensity of 250 W/cm^2 for this sample which is the lowest reported value for the AlGaAs-GaAs materials system[3]. At 752 W/cm^2 no well resolved exciton resonances are discernible in the spectrum of Fig. 8. The continuum spectrum is saturated at 7520 W/cm^2. The excitation dependence of the peak absorption feature at about 8500Å is shown in Fig 8b. As will be described in the next section, the saturation behavior can be described by two separate mechanisms [3] that are due to the exciton bleaching and to bandfilling of the continuum states [18]. The excitation behavior of these two mechanisms are indicated by the solid curves below the data. The solid line through the data is the sum of these two mechanisms. The saturation intensity of sample V136 grown at the the highest temperature (750°C) was comparable to the band to band saturation intensity of sample V158. This is to be expected since the high carrier concentration in sample V136 resulted in screening of the exciton resonance.

The dependence of the n=1 heavy hole excitonic absorption coefficient under resonant excitation for the MQW samples with different well widths is shown in Fig. 9. The saturation mechanism in each case can described by a two component saturation similar to the data of Fig. 8. The magnitude of the absorption attributed to the excitonic resonance is observed to decrease with increasing well width. The background continuum absorption is observed to decrease somewhat more slowly than the excitonic component with increasing well width. These trends are the result of the decreasing density of available

band edge states associated with the first allowed level and the decreased binding energy of the exciton as the well width is increased. The measured saturation intensity for the excitonic and background component is listed in Table 3. Proper interpretation of these measurements must take into account the minority carrier lifetime of the samples. This will be addressed in the next section.

The measured saturation behavior of the light hole resonance and the higher energy (E_{hh} +50 meV) continuum band edge states for the sample with 54 Å wells is shown in Fig.10 a&b. A two component saturation is seen for the light hole resonance whereas the continuum band edge absorption showed only one component as expected. This behavior is observed for the 72Å and 102Å well samples but the light hole resonance could not be resolved for samples with thicker wells. The saturation intensities for the resolvable light hole resonances and the band to band transitions are shown in Table 3. The saturation intensity of the light hole resonance is uniformly higher than the heavy hole saturation intensity. This is to be expected from the ratio of the effective masses.

VI. Analysis of Nonlinear Absorption Properties

Saturation Intensity

The mechanism for saturation of the excitonic absorption features in multiple quantum wells has been studied in some detail. Resonant excitation with picosecond pulses has conclusively shown that the exciton formed in the absorption process is thermalized in a few hundred femtoseconds leading to the formation of free electrons and holes [19]. The reduction in oscillator strength then results from the interaction of these free carriers with free exciton states. The primary interactions responsible for bleaching of the excitonic resonance are thought to be screening of the Coulombic interaction and phase space filling [18]. The continuum states that overlap the exciton resonances are saturated by band fillng of the available continuum states . To properly interpret and analyze the data shown in previous section we adopt a phenomonological model for these mechanisms proposed by Chemla and co-workers [20]. The dependence of the absorption coefficient upon excitation is expressed as :

$$\alpha_{exc} = \frac{\alpha^{o}_{exc}}{1 + (I / I_S)} \qquad (2)$$

where α^{o}_{exc} is the low intensity value of the absorption coefficient and I_S is the intensity at which the absorption coefficient is reduced by half, the saturation intensity, given by:

$$I_S = h\upsilon / (2 L_z \alpha^{o}_{exc} \tau A_x). \qquad (3)$$

In (3), L_z is the well width, τ is the minority carrier lifetime, and A_x is the effective area of the exciton. Note that the saturation intensity decreases with increasing well width and minority carrier lifetime. The exciton area has been calculated to be a function of the well width [21]. We will compare the value determined from our measurements with the theory.

Since continuum absorption also contributes to the absorption measured at the exciton resonance, the total absorption is the sum of two components both of which we model with a functional form similar to (1).

$$\alpha_{tot} = \frac{\alpha^{o}_{exc}}{1 + (I / I_{S1})} + \frac{\alpha^{o}_{con}}{1 + (I / I_{S2})} \qquad (4)$$

The background continuum absorption, α^{o}_{con}, is a function of carrier concentration and crystalline perfection. In addition, there may be an unsaturable background absorption detrimental to device operation. In most instances that we have examined $I_{S1} << I_{S2}$, allowing us to determine them from the limiting behavior of the absorption coefficient. In the intensity range wher $I >> I_{S1}$ the effective absorbance is given by the second term of (4), then α^{o}_{con} and I_{S2} can be determined from the slope and intercept of a plot of $1 / \alpha_{tot}$ as a function of I as shown in Fig. 11a for the sample with 102Å quantum wells.

$$\frac{1}{\alpha_{tot}} = \frac{1}{\alpha^{o}_{con} I_{s2}} + \frac{1}{\alpha^{o}_{con}} \qquad (5)$$

In the low intensity range $I_{s1} \leq I << I_{s2}$, the absorption coefficient can be represented by the first term of (4) plus an intensity independent continuum, α^{o}_{con}. Then a plot of $1 / (\alpha_{eff} - \alpha^{o}_{con})$ versus $1/I$ yields the values of α^{o}_{exc} and I_{s1}.

$$\frac{1}{(\alpha_{tot} - \alpha^{o}_{con})} = \frac{1}{\alpha^{o}_{exc} I_{s1}} + \frac{1}{\alpha^{o}_{exc}} \qquad (6)$$

Fig. 11 b shows this analysis for the sample of Fig. 11 a. We have employed this analysis to determine the saturation intensities and low intensity absorption coefficients for the exciton and continuum absorption. These values are listed in Table 3. These same values were used to calculate the theoretical curves of the excitation dependent absorption coefficient for the samples of Fig. 9. The excellent agreement between experiment and data exhibited in this figure provides ample justification for the procedure used and the empirical saturation formula given by (4).

A similar procedure was used to calculate the saturation intensities and peak absorptions for the light hole exciton resonance and the higher energy continuum states. In the latter case there was often some residual excitonic absorption present due to the continuum states of the exciton. These values are also listed in Table 3.

The peak absorption coefficient for the n=1 heavy hole exciton resonance is plotted as a function of the well width in Fig. 12. Note that the peak absorption increases monotonically with decreasing well width. This is to be expected since the exciton binding energy increases with decreasing well width. The background continuum absorption at the exciton resonance also increases with decreasing well width. Since the density of continuum band edge states

increases as the well width decreases, we would expect that any band tails associated with these states would also increase. However, this component is found to be more erratic and its variation may reflect a varying perfection of the samples used in this study.

Minority Carrier Lifetime and Diffusion Effects

The minority carrier lifetime, τ, controls the concentration of free carriers that are present at a given excitation. The denisty of free carriers in a uniformly excited materials is pr portional to $I\tau$ and the lateral diffusion in a locally excited material is controlled by the diffusion length, $L = (D\,\tau)^{1/2}$. The saturation mechanisms of interest in this work are dependent upon the concentration of free carriers. As a result it is of interest to understand the dependence of τ upon excitation and the structural properties of the MQW materials. We construct here a simplified model for the minority carrier lifetime that includes both radiative and saturable non-radiative processes to assess the effects of excitation on Δn, the excess free carrier concentration.

We consider steady state conditions to coincide with the quasi-CW excitation used in our saturation experiments. The relevant kinetic equations for the free electron concentration and the saturable non-radiative processes have been solved to yield the following relationship for the minority carrier lifetime:

$$\frac{1}{\tau} = Bp + \frac{1}{\tau_{ns}} + \frac{1}{\tau_c}\ \frac{1}{1 + (\sigma_n \Delta n) / (\sigma_p p)} \qquad (7)$$

The first term is the raditive lifetime, where B is the radiative coeffecient and p is the free hole concentration. The second term is the non-saturable non-radiative lifetime due to deep recombination centers. The final term is a saturable nonradiative lifetime due to recombination centers that can be filled by capturing excess electrons (i.e. $\sigma_n >> \sigma_p$) where the σ's are the capture cross sections for electrons and holes. This equation has been written assuming that electrons are the minority carriers. An analogous equation for holes could be written in the case electrons are the majority carriers by reversing the n an p. For lightly doped samples as we have here, the radiative term is usually negligible at low excitation and the lifetime is the reciprocal sum of τ_{ns} and τ_c. At higher excitation the final term saturates and the lifetime becomes τ_{ns}.

becomes τ_{ns}. Under conductivity modulation ($p=\Delta p=\Delta n$), the lifetime becomes the reciprocal sum of $(B\Delta n)^{-1}$ and τ_{ns}. We have observed this behavior in the time decay of the samples used in this study and discussed the manifestations of it in Section IV. The task we face here is to decide which regime to use to analyze the saturation data of Table 3. The decays of samples with relatively short minority carrier lifetimes showed no evidence of a fast initial component. The lifetimes of all samples were completely saturated at the maximum intensity available in the lifetime measurement and were independent of intensity over a factor of four in excitation below that. We assume that measured decay time in these cases is the appropriate lifetime to use in this analysis. We recognize that the radiative component may become important at higher excitations near the point of absorption saturation. We estimate that for a free carrier concentration of $\Delta n = 10^{17}$ cm^{-3} the radiative lifetime will be of the order 100-200 nsec. This is based on our observation of the excitation dependence of the time decay measured on very long lifetime samples and other data in the literature [22]. Our lifetimes were measured with an impulse excitation that generates approximately 10^{16} cm^{-3} carriers. We are clearly in the regime where radiative processes may be important in the determination of the saturation intensity. In fact, for very efficient materials (*i.e.* $\tau_{ns} >> (B\Delta n)^{-1}$), photon reabsorption may artificially lengthen the lifetime and lower the saturation intensity.

The long minority carrier lifetimes we measure in this study result in diffusion lengths comparable to the effective spot diameters used in the saturation measurements. Recent work by Olsson et al. [23] suggests that the effective spot size must be corrected to include the outdiffusion of carriers. The effective saturation intensity is then calculated from:

$$I_{eff} = P_S / (4\pi D\tau + A_{spot}) \qquad (8)$$

where P_S is the saturation power. This correction has the effect of increasing the spot size dramatically for the sample with the longest lifetime. We have used a diffusion constant D = 17 cm^2/sec [23] to account for ambipolar diffusion of the carriers. The corrected saturation intensities are shown in Table 3. These data show that very low saturation intensities are possible at the peak of the

exciton resonance if suitable carrier confinement can be included in the device structure.

Saturation Density and Exciton Radius

Based on the measured saturation intensities, measured lifetimes and measured absorption coefficients we can calculate the saturation density of carriers defined by :

$$n_S = \frac{I_S \tau \alpha(I_S)}{h\nu} \qquad (9)$$

The saturation density n_S is the density of photogenerated carriers that reduces the excitonic component of the absorption coefficient to one half of its low intensity value. Fig. 13a shows the dependence of n_S upon well width. The saturation density shows a broad maximum in the range L_Z = 100Å. We believe the apparent maximum is shifted to larger well widths by the data point at 133Å. This sample is believed to have spuriously high saturation intensity. It is the only sample that exhibited a smaller minority carrier lifetime in the fabricated absorption sample than in the bulk sample. In addition, the measured lifetime of the absorption sample does not follow the trend observed in the other samples. On the other hand no visble physical damage is present and we have included the sample data for completeness. In view of these considerations, we believe that the maximum saturation density is near L_Z =75Å. This can be understood if we realize that:

$$A_{ex} L_Z \approx 1/2n_S \qquad (10)$$

The exciton radius calculated from (10) by assuming $r_{exc} = (A_{exc}/\pi)^{1/2}$ is plotted in Fig. 13b. Note that r_{exc} reaches a minimum near L_Z =75Å and increases on either side. This behavior is a reflection of the increased confinement of the exciton as the well is decreased up to the point that the wave functions of the carriers begin to significantly overlap the barrier regions. This is expected to occur in the range L_Z= 75Å. It must be pointed out that although the exciton is not spherically symmetric [24], its dimension along the layers also contracts as the transverse dimension is increasingly confined. The quantity A_{ex} increases with decreasing well width for samples with the smallest well widths while L_Z decreases. As a result, the saturation density, n_S,

proportional to $(A_{ex} L_z)^{-1}$, is weakly dependent upon the well width. For the widest wells, A_{ex}^{-1}, L_x^{-1}, and n_s, are all small.

VII. Alternate Structure for Photonic Switches

A major technological difficulty in the fabrication of arrays of photonic switches in the AlGaAs/ GaAs system is the opacity of the GaAs substrate. Jewel et al. [25] and Boyd et al. [26] have demonstrated photonic switches that contain internal mirrors based on epitaxial Bragg reflectors. Fig 14 shows the reflection spectrum of one such reflector grown by MOCVD. The layer thickness of this structure was chosen to maximize the reflectance in the spectral region near the excitonic resonances in GaAs quantum wells. Note that this reflector has a 600Å bandwidth and a maximum reflectivity of 0.96. The structure contains 30 periods of AlAs/$Al_{0.2}Ga_{0.8}As$ each layer being a quarter wavelength thick. The use of such a high reflectivity mirror isolates the device from the substrate and provides a double pass through the active region. This has been put to use in reflective modulator devices to improve the contrast ratio [26]. The major difficulty with this approach is the resultant requirement to use the device in a reflective mode.

We have recently demonstrated an alternate approach to photonic switch technology by the growth of AlGaAs/ GaAs MQW structures on transparent GaP substrates [27]. The large lattice mismatch of the substrate and the active layers has been accommodated by interposing a $GaAs_{0.6}P_{0.4}$ buffer layer between the active region and the GaP transparent substrate. The resultant MQW structures show a high degreee of structural perfection, smooth layer morphology and a well resolved excitonic resonance. These structures exhibit very high saturation intensities and are likely not suitable for use as nonlinear optical materials. However, they can be incorporated into PIN electroabsorption modulators that utilize the QCSE[27]. The absorption spectrum of one such modulator is shown in Fig 15 at various applied voltages. Note the shift of the resonance to lower energy that is characteristic of the quantum confined Stark effect [7]. The energy shifts observed in this modulator compare favorably with results obtain on GaAs substrates.

VIII Discussion and Conclusions

We have reported the dependence of the nonlinear absorption coefficient in AlGaAs/GaAs multiple quantum wells grown by MOCVD. The results presented clearly show that MOCVD is a suitable technique for the growth of these nonlinear materials. In fact the low saturation intensities we have observed promise to open new applications for these materials in nonlinear waveguide switches that do not rely upon a high density of switches. In particular we have demonstrated that the saturation intensity of MOCVD grown materials are currently controlled by the minority carrier lifetime in the materials and to some extent by the quantum well structure chosen. Even though the saturation intensities for the heavy hole resonance of AlGaAs/GaAs MQW's demonstrated in this paper are among the lowest ever reported for this materials system, the systematic dependence of this quantity as a function of the well width suggests that fine tuning of the quantum well design can improve the performance of these materials. In particular, it appears that the saturation intensity in the samples investigated to date decreases with increasing well width largely because the minority carrier lifetime increases. The dependence of τ on well width is not thought to be fundamental but rather a result of the quality of the AlGaAs barrier layers presently available. In this context it is perhaps not surprising that InP/InGaAs MQW samples have exhibited somewhat lower saturation intensities [28]. Two key points in assessing the minimum possible saturation intensity are related to the minority carrier lifetime. First, longer minority carrier lifetime causes more lateral diffusion of the photoexcited carriers that affects the apparent saturation intensity. In quasi-CW applications this suggests that some form of lateral carrier confining structure will be necessary to obtain optimum performance. For short pulse applications the relevant quantity is the saturation energy fluence, $I_{sat}\tau$. This quantity is plotted in Fig. 16. Note that the saturation energy fluence has a maximum near a well width of 75Å.The exciton radius is a minimum and, as a result, the saturation density is a maximum in this region. It is thus advisable to design nonlinear materials with L_z away from this maximum for short pulse applications.

The second point to be made is that radiative processes have been largely ignored in the analysis of saturation intensities. As the quality of AlGaAs

improves. MQW's are less likely to be limited by ihe AlGaAs quality and the minority carrier lifetime will ultimately be limited by the radiative processes. At present little is known experimently of the radiative recombination coefficient, B, in MQW structures. As the quality of these structures improves knowledge of this parameter increases in importance.

The technology of photonic switch arrays has been complicated by the necessity of using opaque GaAs substrates on which to grow the MQW epitaxial structures. Selective removal of the substrate requires the use of a fragile, thinned substrate of an already brittle material. This, in turn, will ultimately limit the size of arrays usable in photonic switches and increase their cost. The use of a transparent substrate such as GaP or sapphire may alleviate this difficulty. The encouraging electroabsorption results we have observed in MQW structure grown on GaP strongly suggest that this approach will play an important role should the technology of AlGaAs/GaAs MQW optoelectronic switches be incorporated into practical systems. The success of this approach and the availability of high reflectivity Bragg reflectors gives the system designer a greater measure of flexibility in the design of the system configuration.

This work was supported in part by funding from the Air Force Office of Scientific Research, the National Science Foundation , the Army Research Office, and NASA Lewis Research Center.

REFERENCES

[1] R. Dingle, "Confined Carrier Quantum States in Ultrathin Semiconductor Heterostructures," in Festkörperprobleme (Advances in Solid State Physics), edited by H. J. Queisser (Pergamon, New York 1975), vol. XV, pp. 21-48.

[2] D. S. Chemla and D. A. B. Miller, "Room-temperature excitonic nonlinear optical effects in semiconductor quantum-well structures," *J. Opt. Soc. Amer.*, vol. B2, pp. 1155-1173, 1985.

[3] D. A. B. Miller, D. S. Chemla, D. J. Eilenberger, P. W. Smith, A. C. Gossard and W. T. Tsang, "Large Room-Temperature Optical Nonlinearity in GaAs/$Ga_{1-x}Al_xAs$ Multiple Quantum Well Structures," *Appl. Phys. Lett.*, vol. 41, pp. 679-681, 1982.

[4] J. S. Weiner, D. S. Chemla, D. A. B. Miller, H. A. Haus, A. C. Gossard, W. Wiegmann, and C. A. Burrus, "Highly anisotropic optical properties of single quantum well waveguides," *Appl. Phys. Lett.*, vol. 47, pp. 664-667, 1985.

[5] T. Venkatesan, B. Wilkens, Y. H. Lee, M. Warren, G. Olbright, H. M. Gibbs, N. Peyghmbarian, J. S. Smith, and A. Yariv, "Fabrication of arrays of GaAs optical bistable devices," *Appl. Phys. Lett.*, vol. 48, pp. 145-147, 1986.

[6] D. A. B. Miller, D. S. Chemla, T. C. Daman, A. C. Gossard, W. Wiegmann, T. H. Wood, and C. A. Burrus, "Bandedge electroabsorption in quantum well structures: The quantum confined stark effect," *Phys. Rev. Lett.*, vol. 53, pp. 2173-2177, 1984.

[7] D. A. B. Miller, D. S. Chemla, T. C. Daman, T. H. Wood, C. A. Burrus, A. C. Gossard, and W. Wiegmann,"The quantum well self-electrooptic effect device: Optoelectronic bistability and oscillation, and self-linearized modulation," *IEEE J. Quantum Electron.*, vol. QE-21, pp. 1462-1476, 1985.

[8] H. M. Gibbs, Optical Bistability: Controlling Light with Light, Academic, Orlando, 1985.

[9] P. Daniel Dapkus, "Metalorganic Chemical Vapor Deposition," *Ann. Rev. Mat. Sci.*, vol 12, pp. 243-269, 1982.

[10] James J. Coleman and P. Daniel Dapkus, "Metalorganic Chemical Vapor Deposition," in *Gallium Arsenide Technology* , D. K. Ferry, Ed., Howard W. Sams & Co., Indianapolis, 1985 pp. 79-106.

[11] R. D. Dupuis, L. A. Moudy, and P. D. Dapkus, "Preparation and Properties of AlGaAs-GaAs heterojunctions grown by metalorganic chemical vapor deposition," in *Gallium Arsenide and Related Compounds 1978* , C. M. Wolfe ,Ed., Institute of Physics Conf. Series No. 45, Bristol UK 1978,pp. 1-9.

[12] S. P. Denbaars, H. C. Lee, A. Hariz, and P. D. Dapkus, "Effects of hydrodynamics, interrupted growth and growth temperature on the interface properties of AlGaAs/GaAs quantum wells grown by metalorganic chemical vapor deposition," N-3, Electronic Materials Conferrence, Santa Barbara, CA, June, 1987.

[13] H. C. Lee, A. Hariz, P. D. Dapkus, A. Kost, M. Kawase, and E. Garmire, "AlGaAs GaAs multiple quantum well nonlinear optical materials grown by metalorganic chemical vapor deposition," H-6, Electronic Materials Conference, Santa Barbara, CA, June, 1987.

[14] R. A. Logan and F. K. Reinhart, "Optical Waveguides in GaAs-AlGaAs Epitaxial Layers," *J. Appl. Phys.*, vol. 44, pp. 4172-4176, 1973.

[15] J. E Fouquet and R. D. Burnham, "Recombination dynamics in GaAs AlGaAs quantum well structures," *IEEE J. Quantum Electron.*, vol. QE-22, pp 1799-1810, 1986.

[16] H. C. Lee, A. Hariz, P. D. Dapkus, A. Kost, M. Kawase, and E. Garmire, "Nonlinear Absorption in AlGaAs GaAs Multiple Quantum Well Structures Grown by Metalorganic Chemical Vapor Deposition," *Appl. Phys. Lett.*, vol. 50, pp. 1182-1184, 1987.

[17] P. D. Dapkus, H. M. Manasevit, K. L. Hess, T. S. Low, and G. E. Stillman, "High purity GaAs prepared from trimethylgallium and arsine" *J. of Cryst. Growth*, vol. 55, pp. 10-23, 1981.

[18] H. Haug and S. Schmitt-Rink, "Basic mecanisms of the optical nonlinearities of semiconductors near the bandedge," *J. Opt. Soc. Amer.*, vol. B2, pp. 1135-1142, 1985.

[19] W. H. Knox, R. F. Fork, M. C. Downer, D. A. B. Miller, D. S. Chemla, and C. V. Shank, "Femtosecond dynamics of resonantly excited excitons in room temperature GaAs quantum wells," *Phys. Rev. Lett.*, vol. 54, pp. 1306-1309, 1985.

[20] D. S. Chemla, D. A. B. Miller, P.W. Smith, A. C. Gossard, and W. Wiegmann, "Room Temperature Excitonic Nonlinear Absorption and Reflection in GaAs/AlGaAs Multiple Quantum Well Structures," *IEEE J. Quantum Electron.*, vol. QE-20, pp. 265-275,1984.

[21] A. Kost, M. Kawase, E. Garmire, H. C. Lee, A. Hariz, and P. D. Dapkus, "Contributions to optical absorption in GaAs AlGaAs multiple quantum wells," in Technical Digest, Optical Society of America 1987 Annual Meeting (Optical Society of America, Washington, D. C., 1987) p. 40.

[22] See for example : B. Leskovar, C. C. Lo, P. Hartig, and K. Sauer, "Photon counting system for subnanosecond flourescence lifetime measurements," *Rev. Sci. Instrum.*, Vol. 47, pp. 1113-1121, 1976.

[23] A. Olsson, D. J. Erskine, Z. Y. Xu, A. Schremer, and C. L. Tang, "Nonlinear Lumineseence and Time-Resolved Diffusion Profiles of Photo-excited Carriers in Semiconductors," *Appl. Phys. Lett.*, vol. 41, pp. 659-661, 1982.

[24] G. Bastard, E. E. Mendez, L. L. Chang, and L. Esaki, "Exciton binding energy in quantum wells," *Phys. Rev.*, vol. B26, pp. 1974-1979, 1982.

[25] J. L. Jewell, A. Scherer, S. L. McCall, A. C. Gossard, and J. H. English, "GaAs AlAs monolithic microresonator arrays," *Appl. Phys. Lett.*, vol. 51, pp. 94-96,

1987.

[26] G. D. Boyd, D. A. B. Miller, D. S. Chemla, S. L. McCall, A. C. Gossard, and J. H. English, "Multiple quantum well reflection modulator," *Appl. Phys. Lett.*, vol. 50, pp. 1119-1121, 1987.

[27] H. C. Lee, K. M. Dzurko, P. D. Dapkus, and E. Garmire, "Electroabsorption in AlGaAs/GaAs multiple quantum well structures grown on GaP transparent substrate," *Appl. Phys. Lett.*, vol. 51, (Nov. 16, 1987).

[28] A. M. Fox, A. C. Maciel, M. G. Shorthose, J. F. Ryan, M. D. Scott, J. I. Davies, and J. R. Riffat, "Nonlinear excitonic optical absorption in GaInAs/InP quantum wells," *Appl. Phys. Lett.*, vol. 51, pp. 30-32, 1987.

Table 1 - Characteristics of MQW Structures

Sample #	V158	V159	V160	V136
Growth Temp (°C)	650	700	750	750
Background Carrier Concentration (cm^{-3})	$6x10^{14}$			$4x10^{16}$
Number of Periods	61	61	61	51
Well Thickness (Å)	100	100	100	100
Barrier Thickness (Å)	100	100	100	100
Al Composition	0.32	0.32	0.32	0.32
E_{hh} (eV)	1.4571	1.4553	1.4588	1.4588
E_{lh} (eV)	1.4659	1.4663		
FWHM (meV)	15.4	18.8	20.8	>20

Table 2 - Characteristics of MQW Structures with Different Well Widths.

Sample #	238	237	240	236	239
Well Width (Å)	54	72	102	133	193
# of Periods	100	67	50	33	20
GaAs Active Layer Thickness (μm)	0.54	0.48	0.51	0.44	0.39
Al Composition	0.32	0.32	0.32	0.32	0.32
Barrier Thickness (Å)	150	100	100	100	100

Table 3 - Summary of Nonlinear Optical Properties of MQW samples with Different Well Widths.

Sample #	238	237	240	236	239
Well Thickness (Å)	54	72	102	133	193
Minority Carrier Lifetime (nsec)	59.5	68.7	205	63.8	624
λ_{hh} (nm)	825	839	854	862.5	870
λ_{lh} (nm)	815	829.5			
λ_c (nm)	797	810	831	860	830
α_{hh}^{ex} (μm^{-1})	1.74	1.41	1.32	0.77	0.61
α_{hh}^{bg} (μm^{-1})	1.16	1.74	1.18	1.14	0.64
α_{lh}^{ex} (μm^{-1})	0.767	1.06			
α_{lh}^{bg} (μm^{-1})	1.90	1.65			
α_{con}^{ex} (μm^{-1})	0.0	.15	0.31	0.35	0.24
α_{con}^{ex} (μm^{-1})	2.35	1.96	0.71	1.24	1.28
Saturation Intensities below measured in kW/cm^2.					
$I_{sat_{hh}}^{ex}$ (measured)	0.321	0.960	0.304	0.697	0.250
$I_{sat_{hh}}^{ex}$ (corr.)	0.062	0.074	0.020	0.128	0.0023
$I_{sat_{hh}}^{bg}$ (corr.)	3.11	26.4	9.00	10.1	1.50
$I_{sat_{lh}}^{ex}$ (corr.)	0.065	0.197			
$I_{sat_{lh}}^{bg}$ (corr.)	3.19	19.3			
$I_{sat_{con}}^{ex}$ (corr.)		0.012	0.10	0.19	0.02
$I_{sat_{con}}^{bg}$ (corr.)	10.3	26.4	3.88	9.67	1.59

List of Figures

Fig. 13 Dependence of the (a) saturation carrier density, n_s, and (b) exciton radius, r_{ex}, as a function of the well width.

Fig. 14 Reflectance spectrum of a 30 period $Al_{0.2}Ga_{0.8}As/AlAs$ Bragg reflector grown by MOCVD.

Fig. 15 Transmission spectrum of AlGaAs/GaAs MQW electroabsorption modulator grown on GaP at various applied voltages.

Fig. 16 The saturation energy fluence, $I_s\tau$, as a function of the well width of AlGaAs/GaAs MQW's.

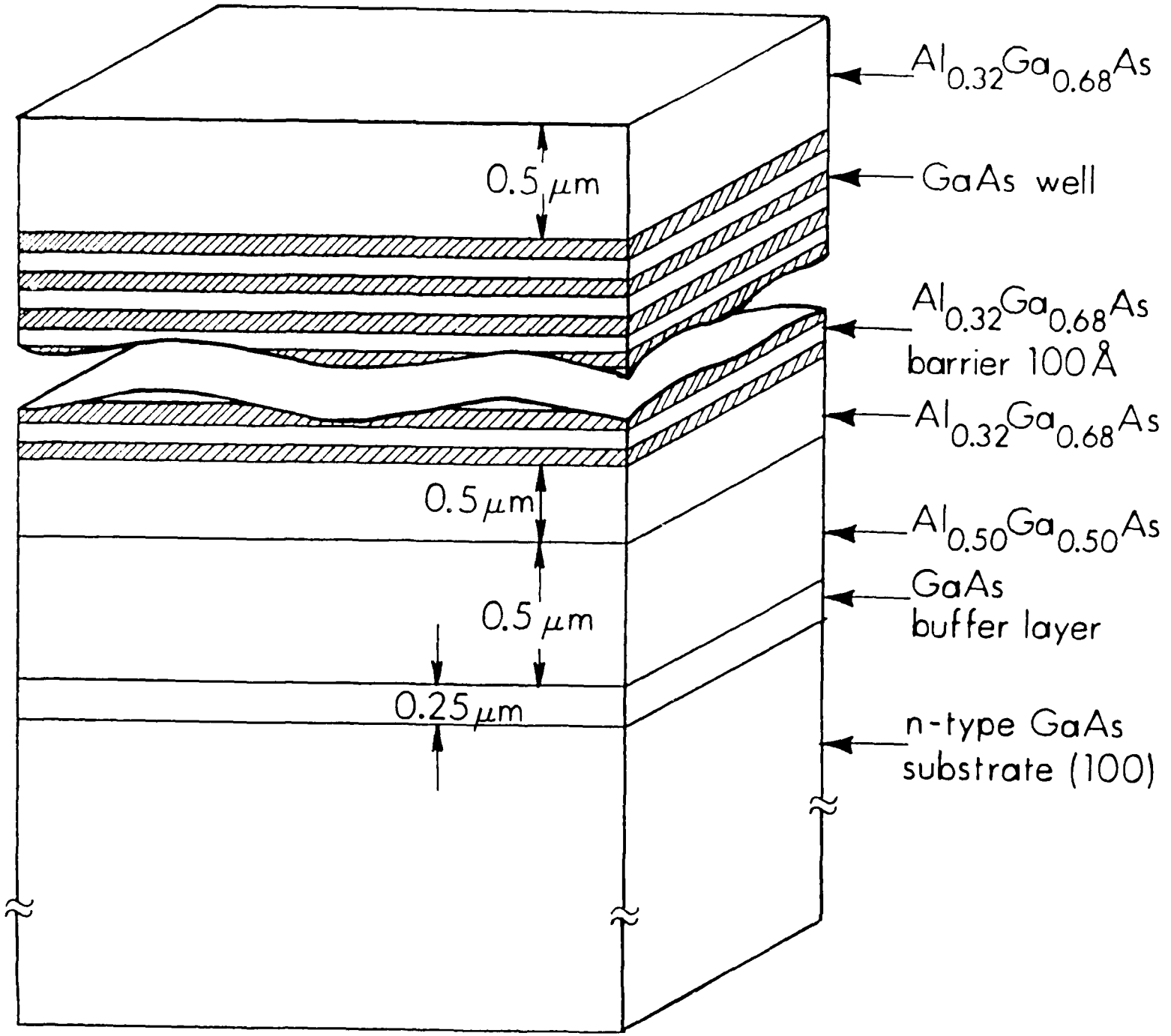
$Al_{0.32}Ga_{0.68}As$
GaAs well
$Al_{0.32}Ga_{0.68}As$
barrier 100 Å
$Al_{0.32}Ga_{0.68}As$
$Al_{0.50}Ga_{0.50}As$
GaAs
buffer layer
n-type GaAs
substrate (100)
0.5 μm
0.5 μm
0.5 μm
0.25 μm

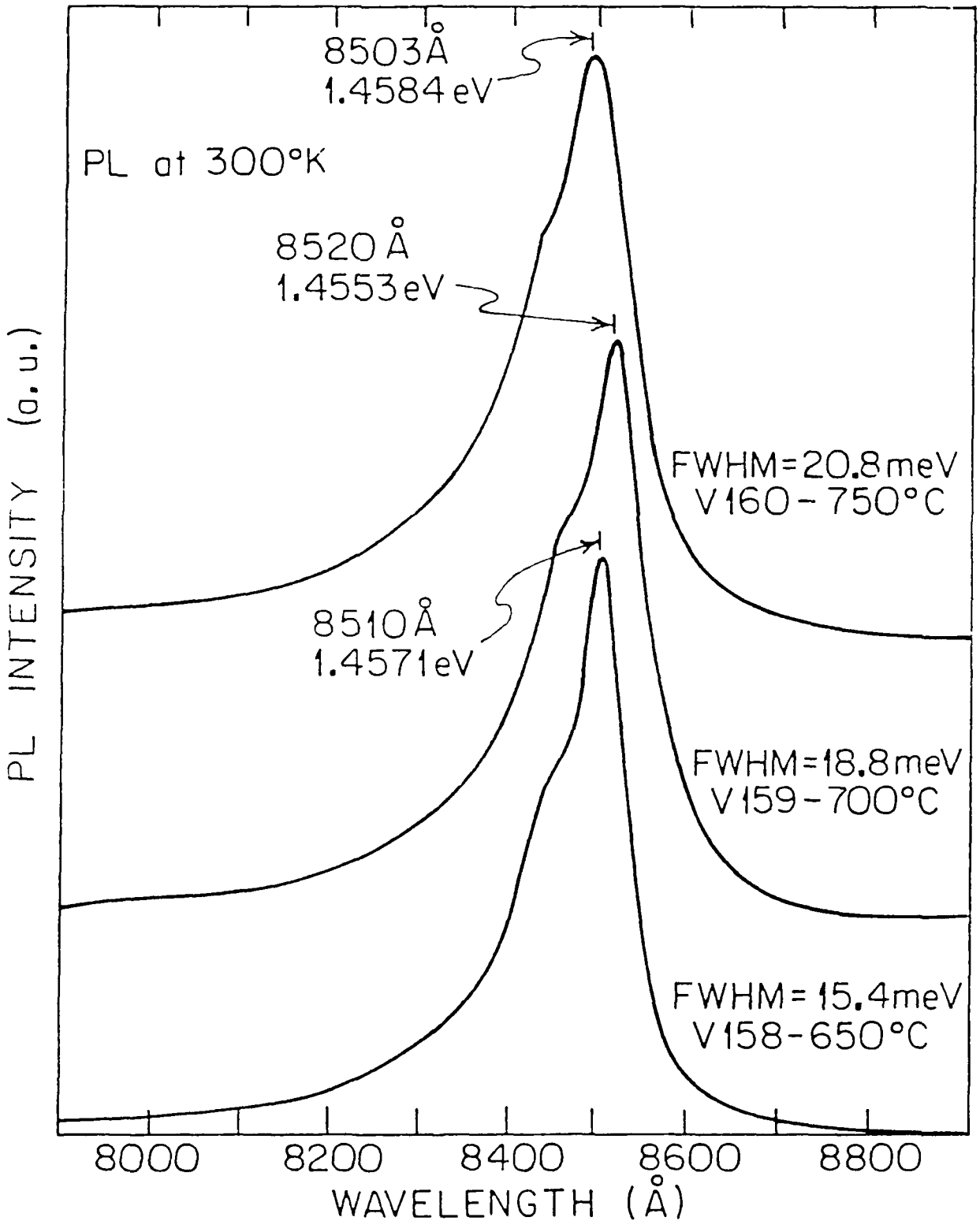
8503Å
1.4584 eV
PL at 300°K
8520 Å
1.4553 eV
FWHM=20.8meV
V160-750°C
8510Å
1.4571eV
FWHM=18.8meV
V159-700°C
FWHM=15.4meV
V158-650°C
PL INTENSITY (a.u.)
8000
8200
8400
8600
8800
WAVELENGTH (Å)

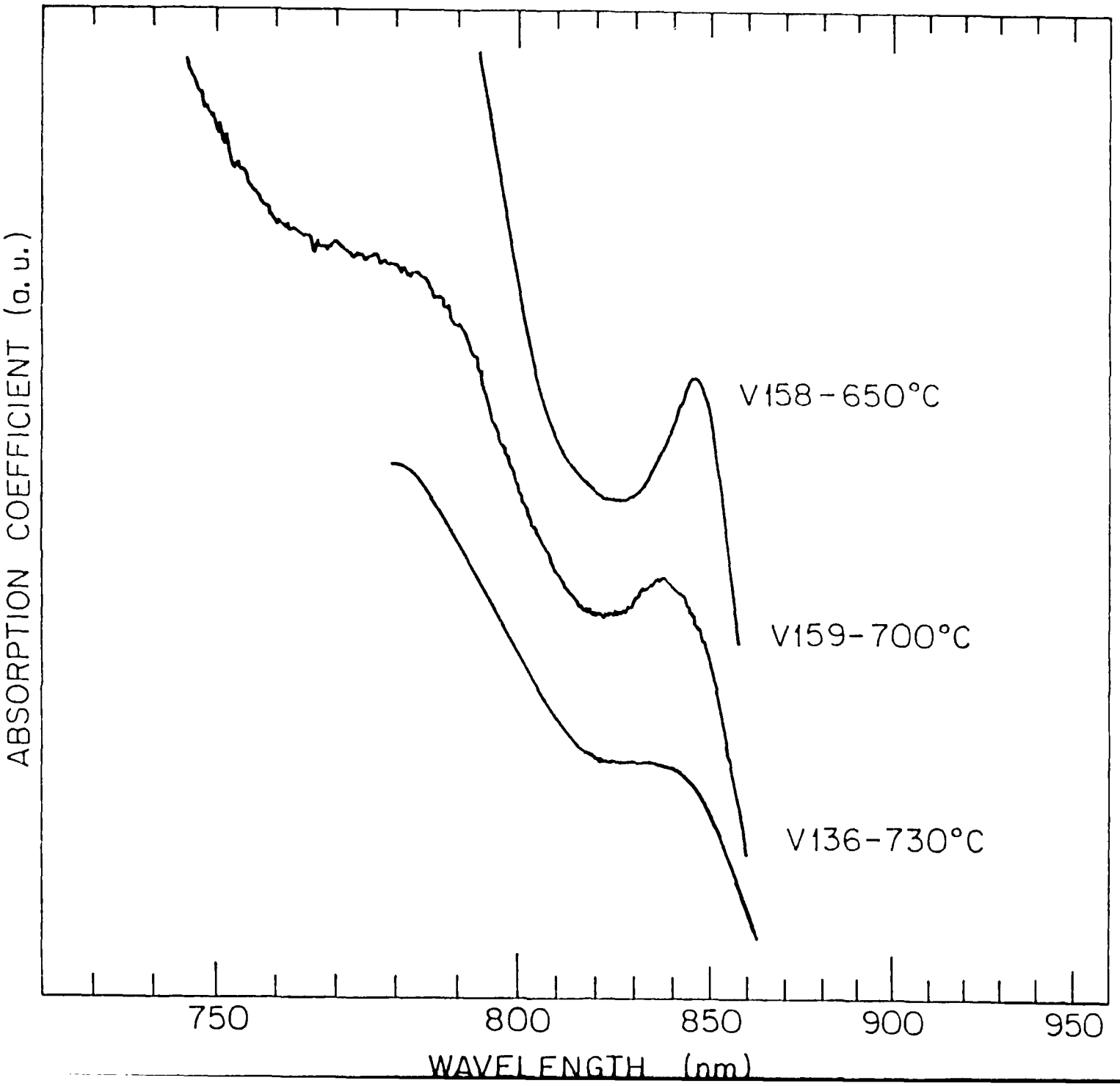
ABSORPTION COEFFICIENT (a.u.)
V158-650°C
V159-700°C
V136-730°C
750
800
850
900
950
WAVELENGTH (nm)

Fig. 3

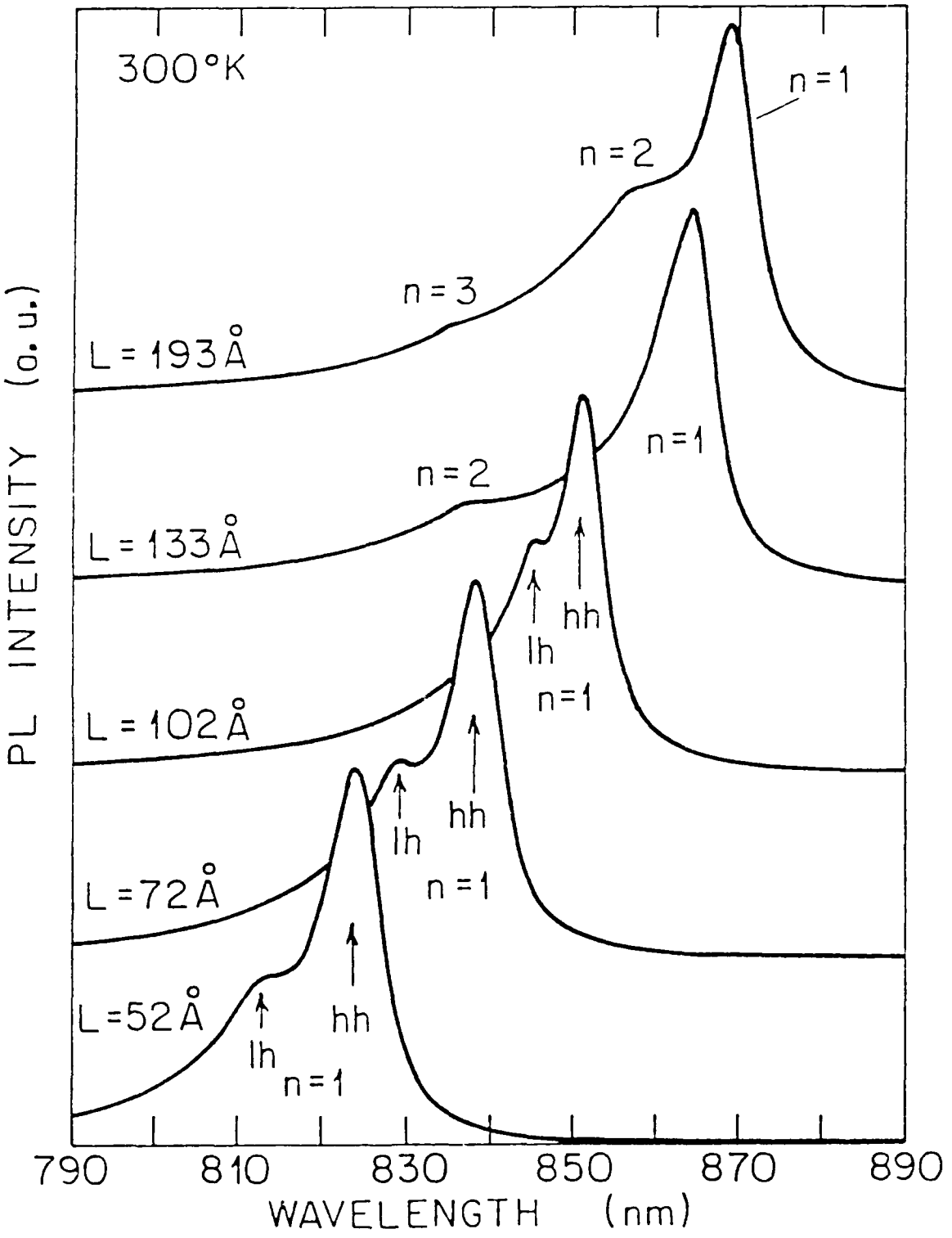
300°K
n=1
n=2
n=3
L=193Å
n=2
n=1
L=133Å
lh
hh
n=1
L=102Å
lh
hh
n=1
L=72Å
lh
hh
n=1
L=52Å
PL INTENSITY (a.u.)
790
810
830
850
870
890
WAVELENGTH (nm)

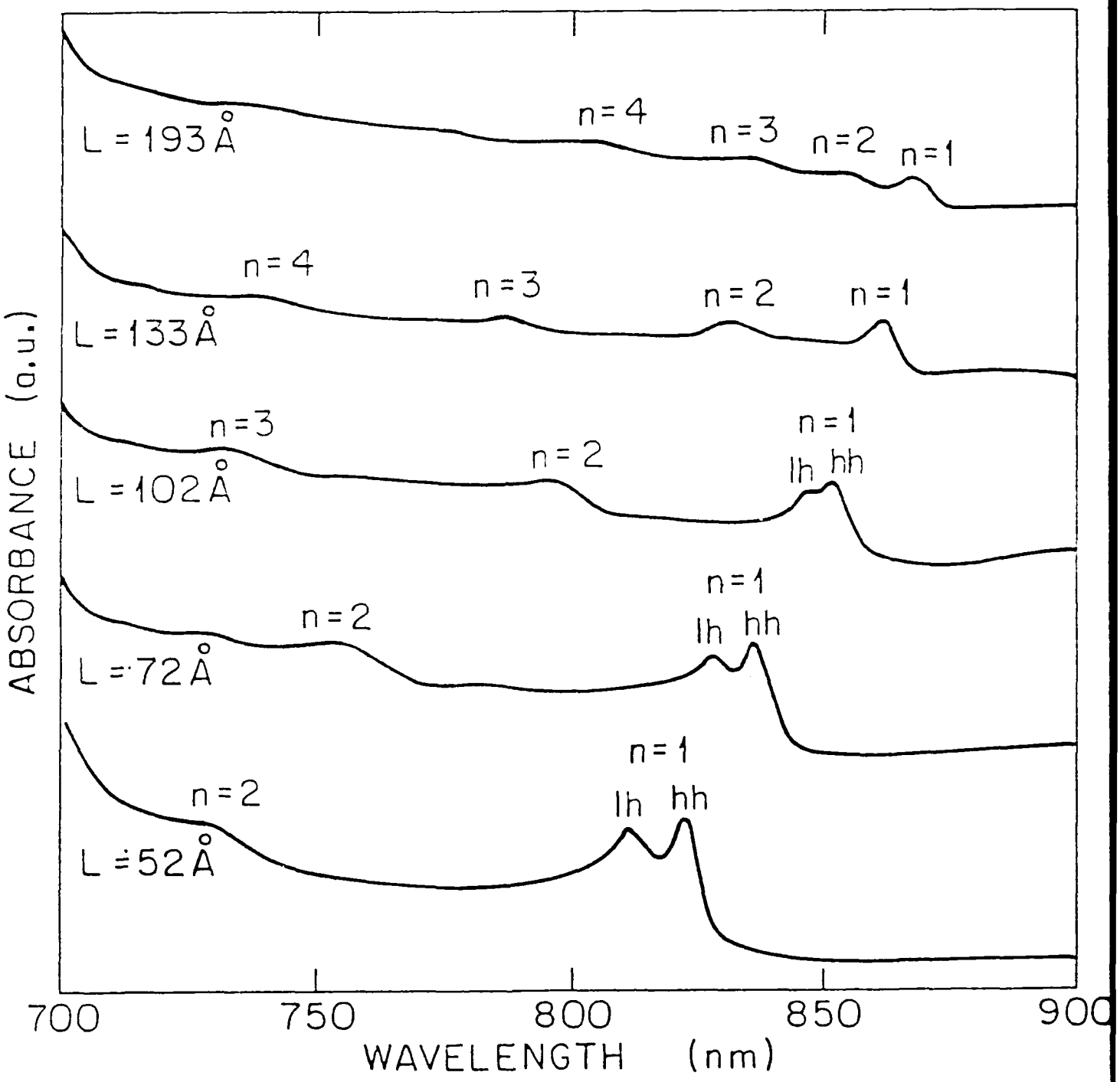
L = 193 Å
n = 4
n = 3
n = 2
n = 1
L = 133 Å
n = 4
n = 3
n = 2
n = 1
L = 102 Å
n = 3
n = 2
n = 1
lh hh
L = 72 Å
n = 2
n = 1
lh hh
L = 52 Å
n = 2
n = 1
lh hh
ABSORBANCE (a.u.)
700
750
800
850
900
WAVELENGTH (nm)

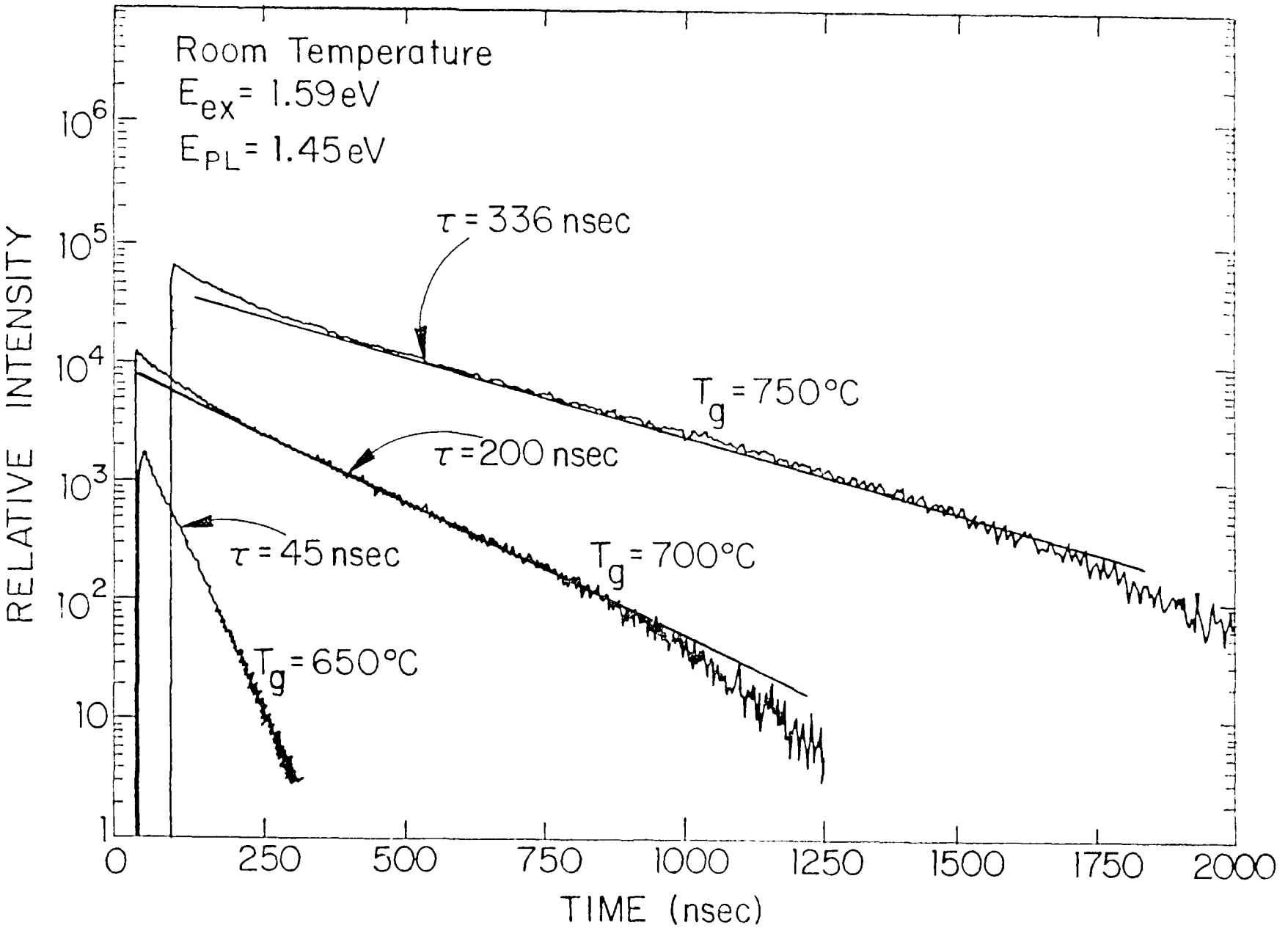
Room Temperature
E_{ex} = 1.59 eV
E_{PL} = 1.45 eV
τ = 336 nsec
T_g = 750°C
τ = 200 nsec
T_g = 700°C
τ = 45 nsec
T_g = 650°C
RELATIVE INTENSITY
10^6
10^5
10^4
10^3
10^2
10
1
0
250
500
750
1000
1250
1500
1750
2000
TIME (nsec)

Fig. 6

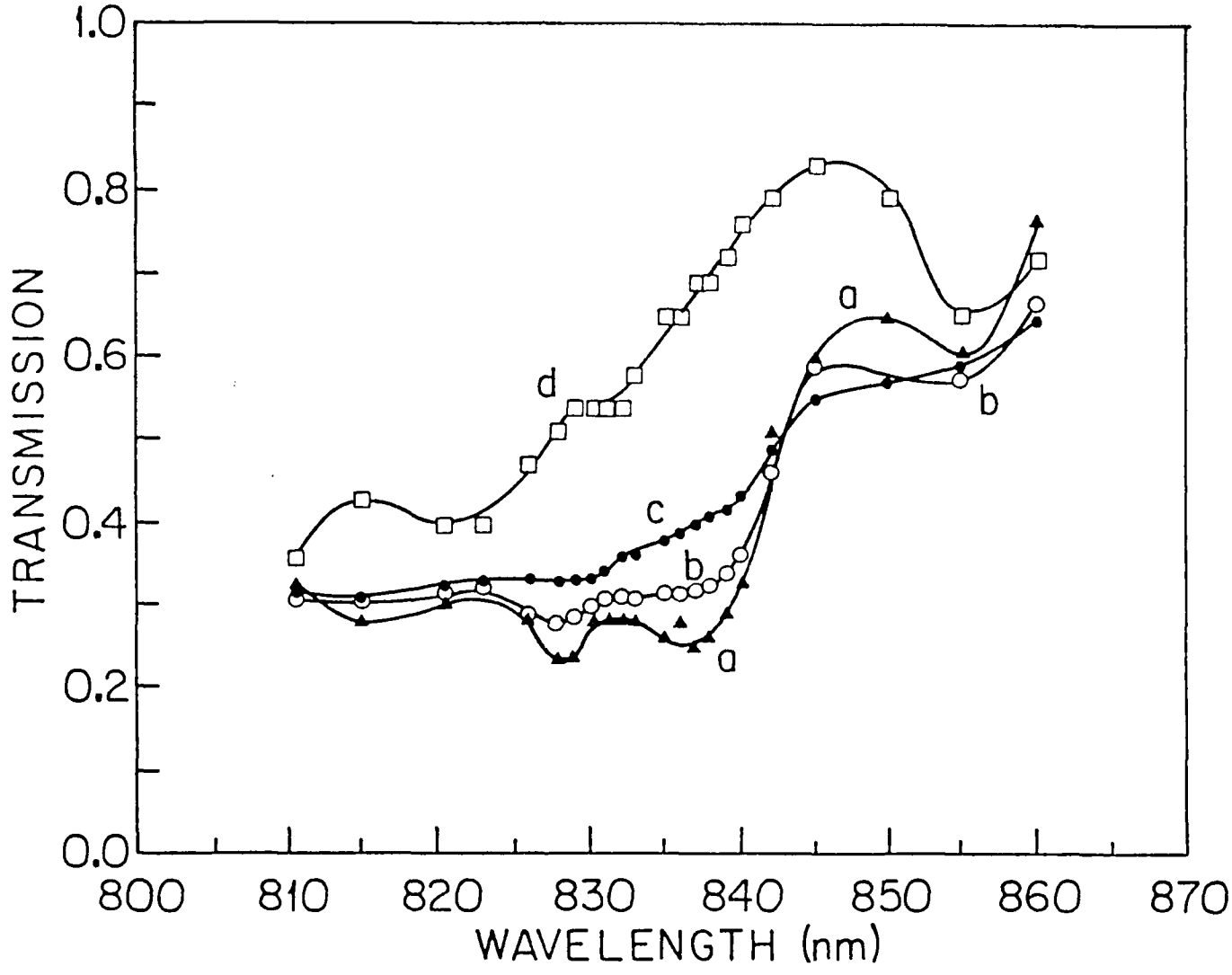
1.0
0.8
0.6
0.4
0.2
0.0
TRANSMISSION
800
810
820
830
840
850
860
870
WAVELENGTH (nm)
a
b
c
d
b
a

Fig. 7 (a)

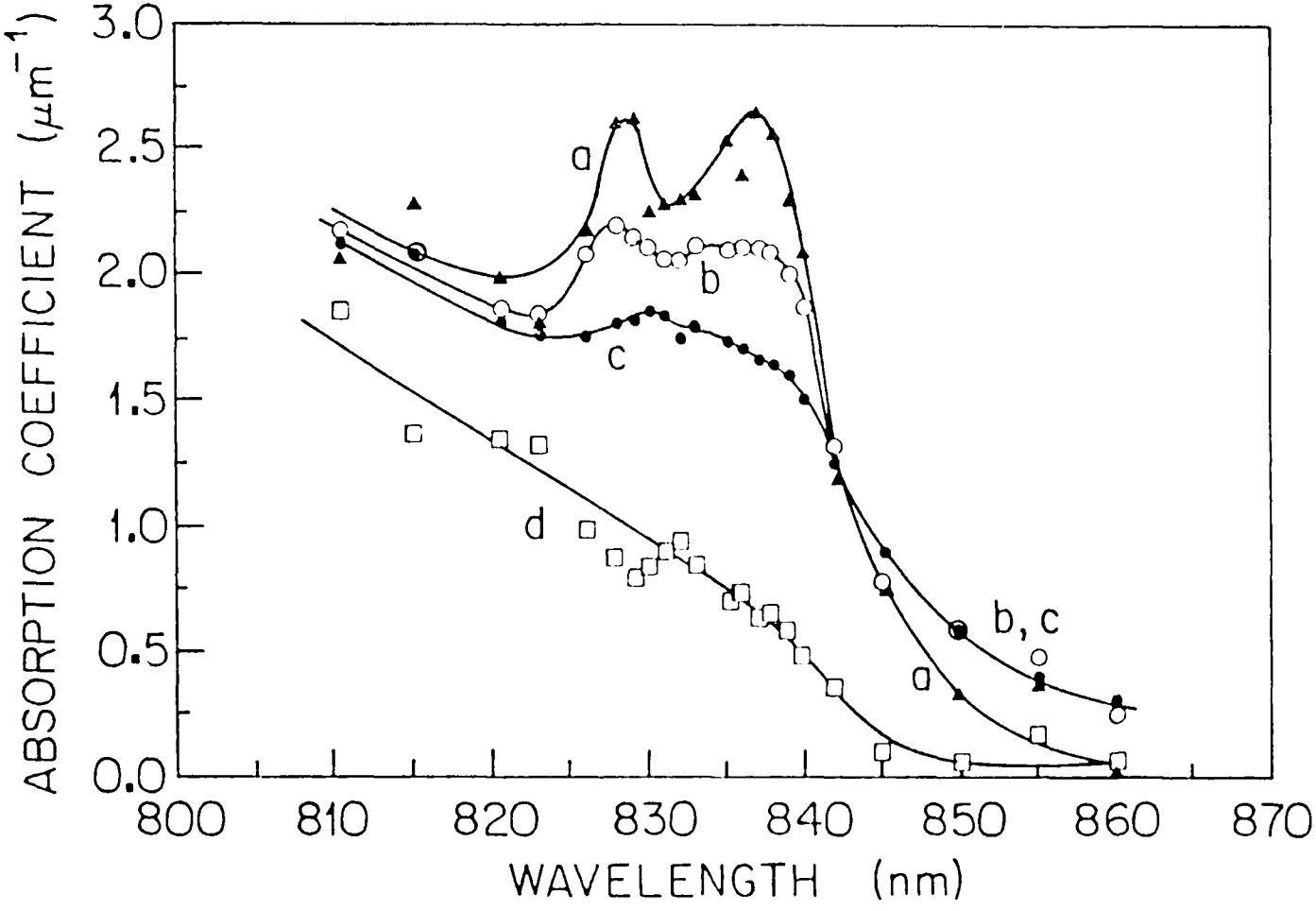
ABSORPTION COEFFICIENT (μm^{-1})
3.0
2.5
2.0
1.5
1.0
0.5
0.0
800
810
820
830
840
850
860
870
WAVELENGTH (nm)
a
b
c
d
b, c
a

Fig. 7 (b)

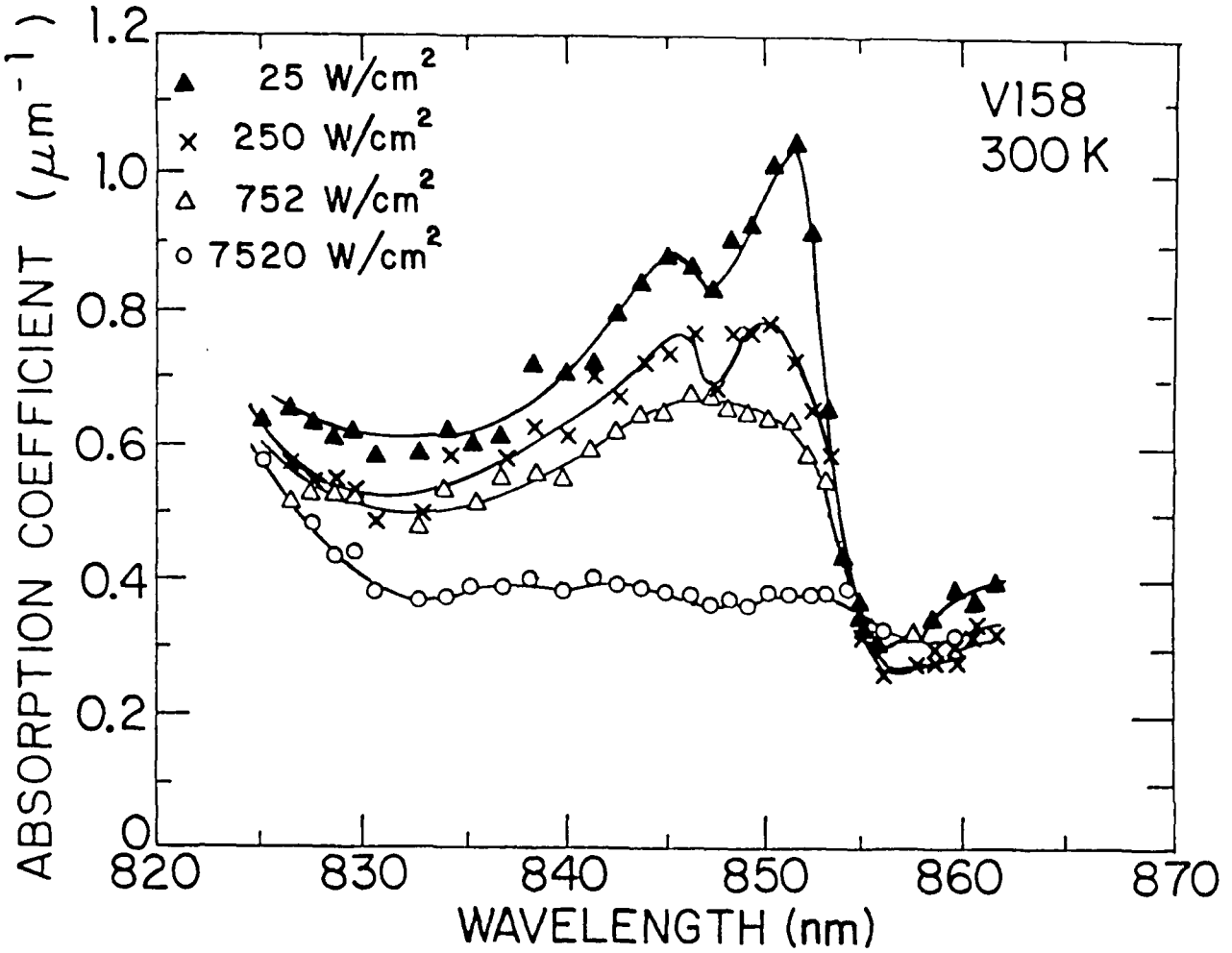
ABSORPTION COEFFICIENT (μm^{-1})
1.2
1.0
0.8
0.6
0.4
0.2
0
820
830
840
850
860
870
WAVELENGTH (nm)
25 W/cm^2
250 W/cm^2
752 W/cm^2
7520 W/cm^2
V158
300 K

Fig. 8 (a)

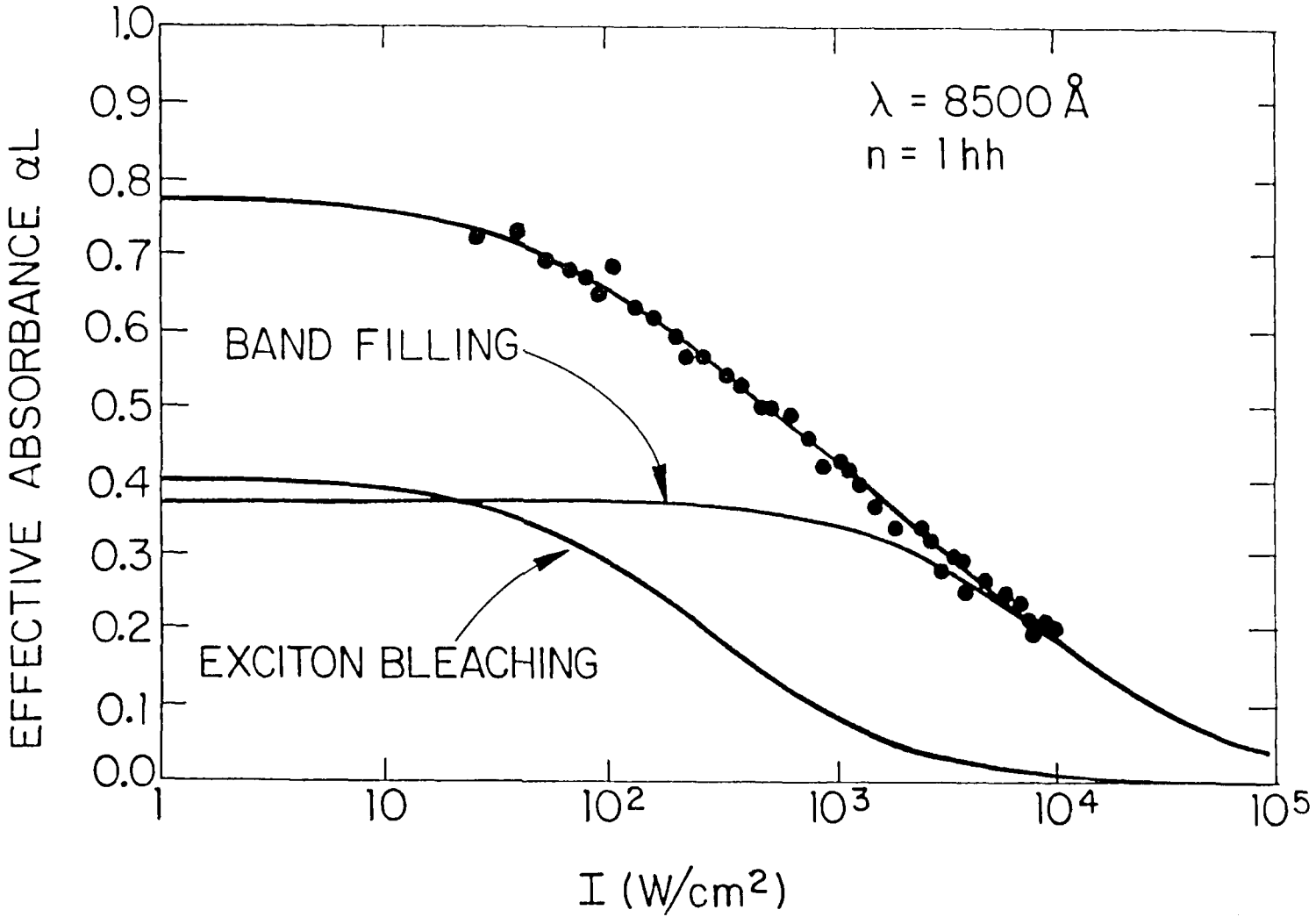
λ = 8500 Å
n = 1 hh
BAND FILLING
EXCITON BLEACHING
EFFECTIVE ABSORBANCE αL
I (W/cm²)
1.0
0.9
0.8
0.7
0.6
0.5
0.4
0.3
0.2
0.1
0.0
1
10
10²
10³
10⁴
10⁵

Fig. 8 (b)

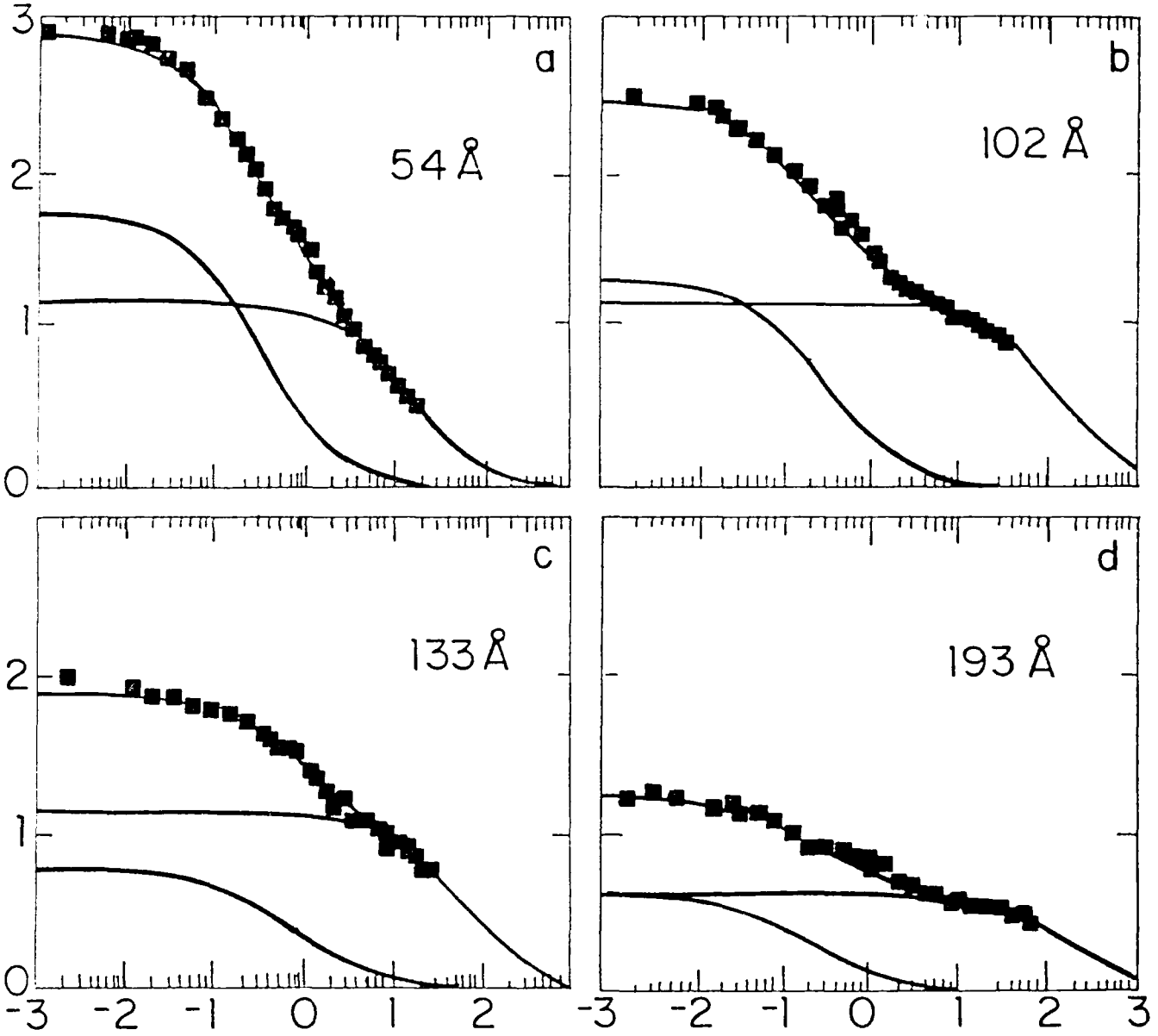

Fig. 9

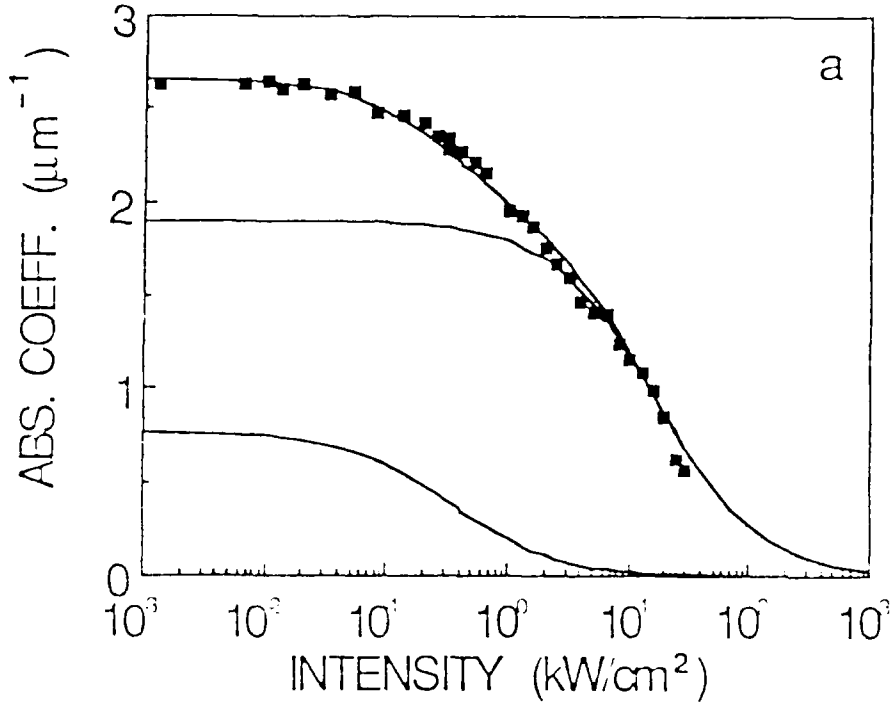
a
ABS. COEFF. (μm⁻¹)
INTENSITY (kW/cm²)
0
1
2
3
10⁻³
10⁻²
10⁻¹
10⁰
10¹
10²
10³

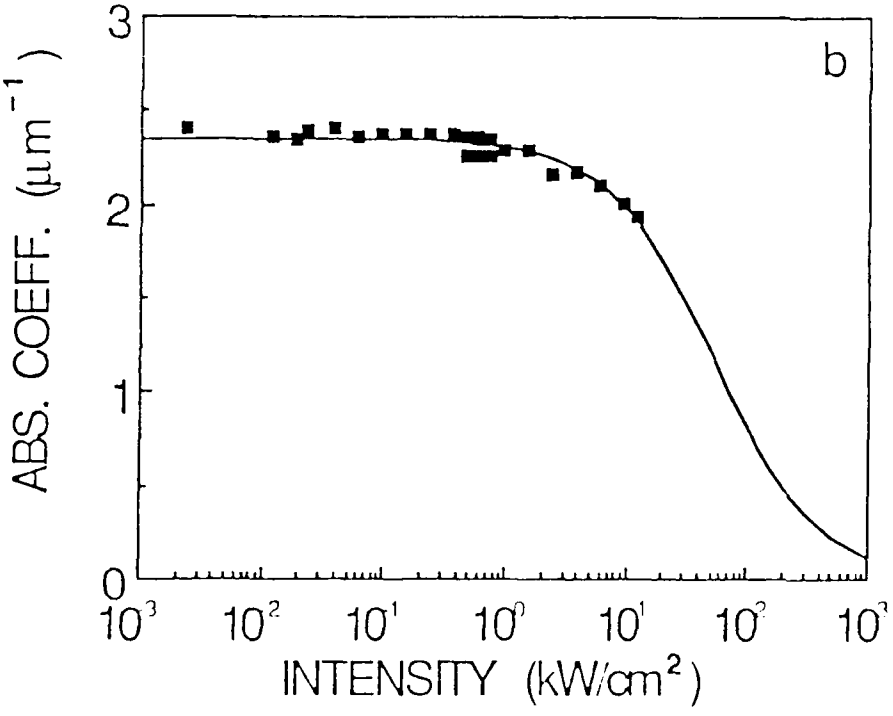
b
ABS. COEFF. (μm⁻¹)
INTENSITY (kW/cm²)
0
1
2
3
10⁻³
10⁻²
10⁻¹
10⁰
10¹
10²
10³

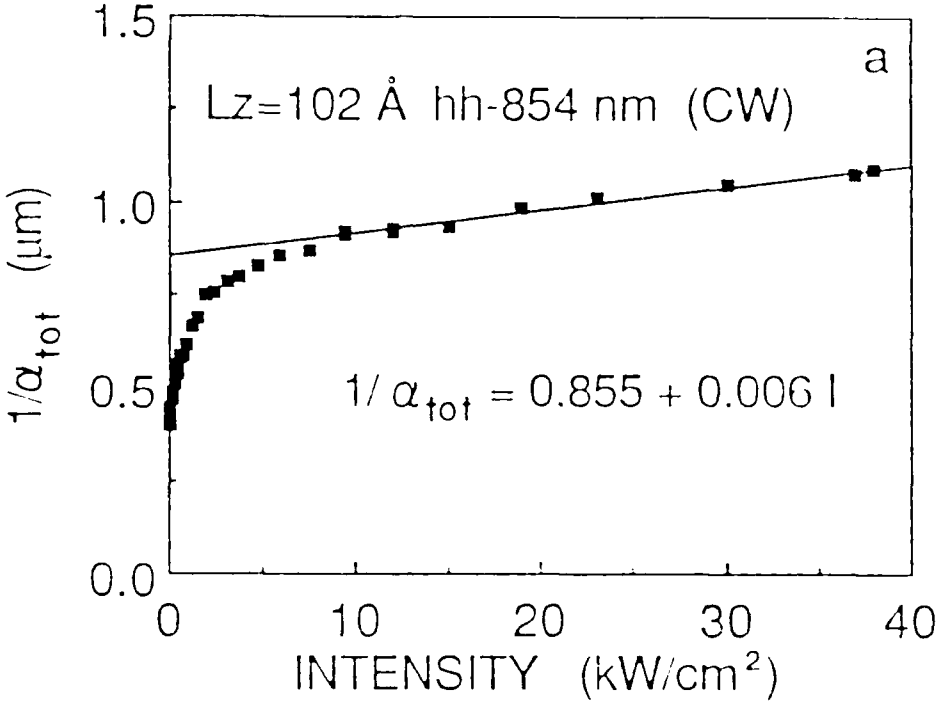
a
Lz=102 Å hh-854 nm (CW)
$1/\alpha_{tot}$ = 0.855 + 0.006 I
$1/\alpha_{tot}$ (μm)
INTENSITY (kW/cm²)
1.5
1.0
0.5
0.0
0
10
20
30
40

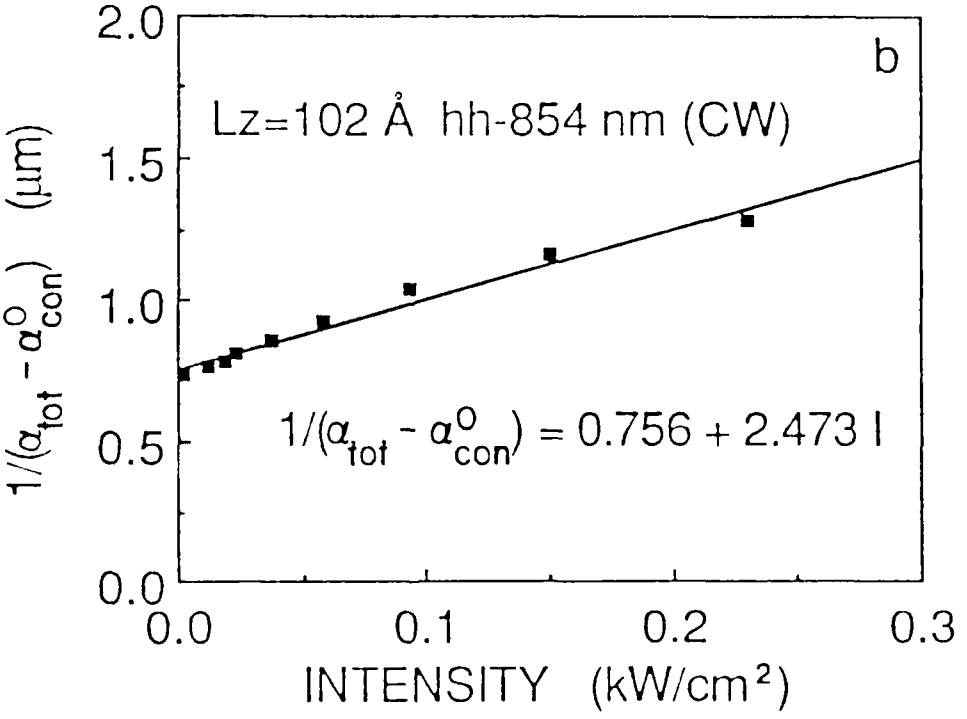
b
Lz=102 Å hh-854 nm (CW)
$1/(\alpha_{tot} - \alpha^0_{con})$ = 0.756 + 2.473 I
$1/(\alpha_{tot} - \alpha^0_{con})$ (μm)
INTENSITY (kW/cm²)
2.0
1.5
1.0
0.5
0.0
0.0
0.1
0.2
0.3

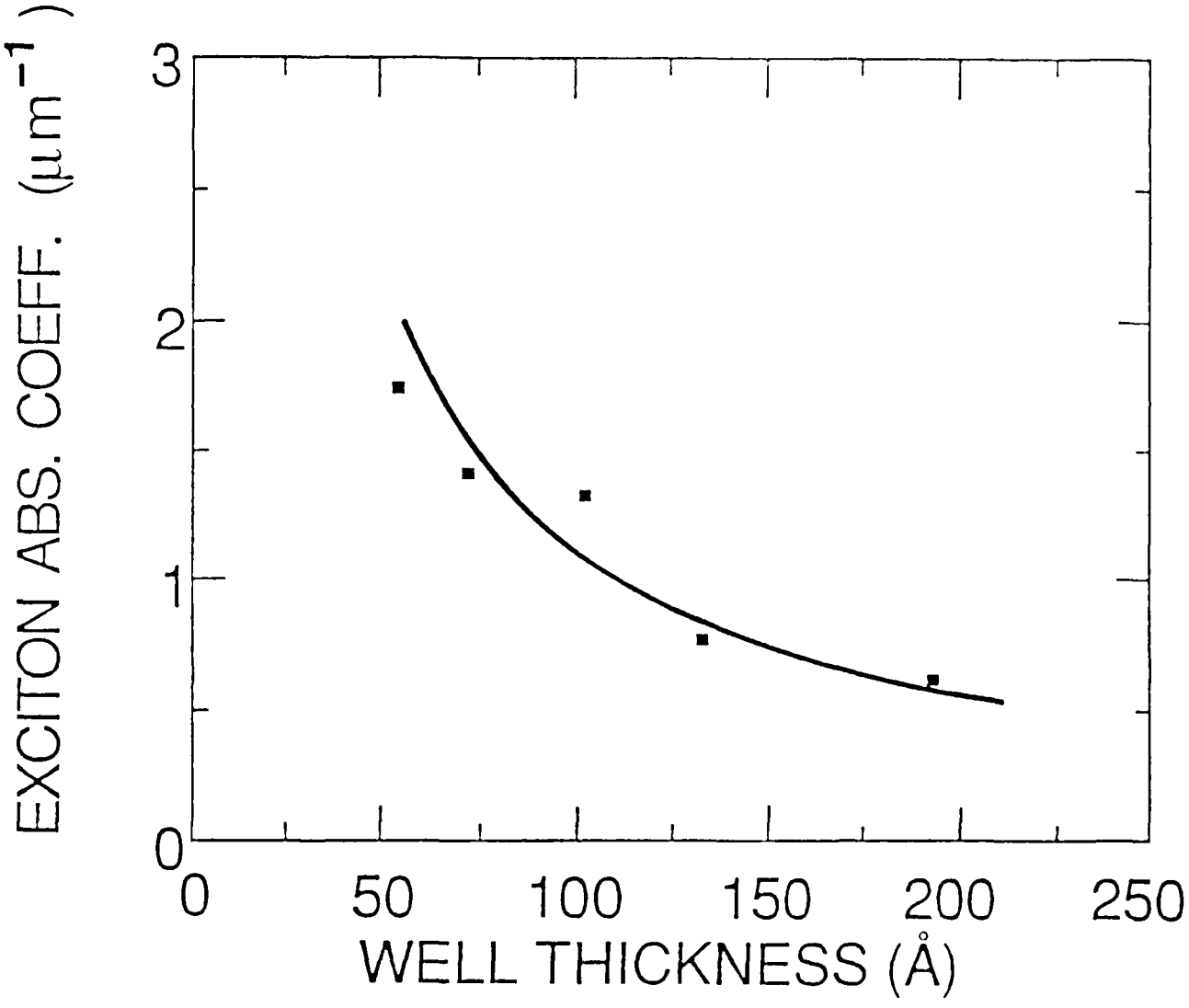
EXCITON ABS. COEFF. (μm⁻¹)
3
2
1
0
0
50
100
150
200
250
WELL THICKNESS (Å)

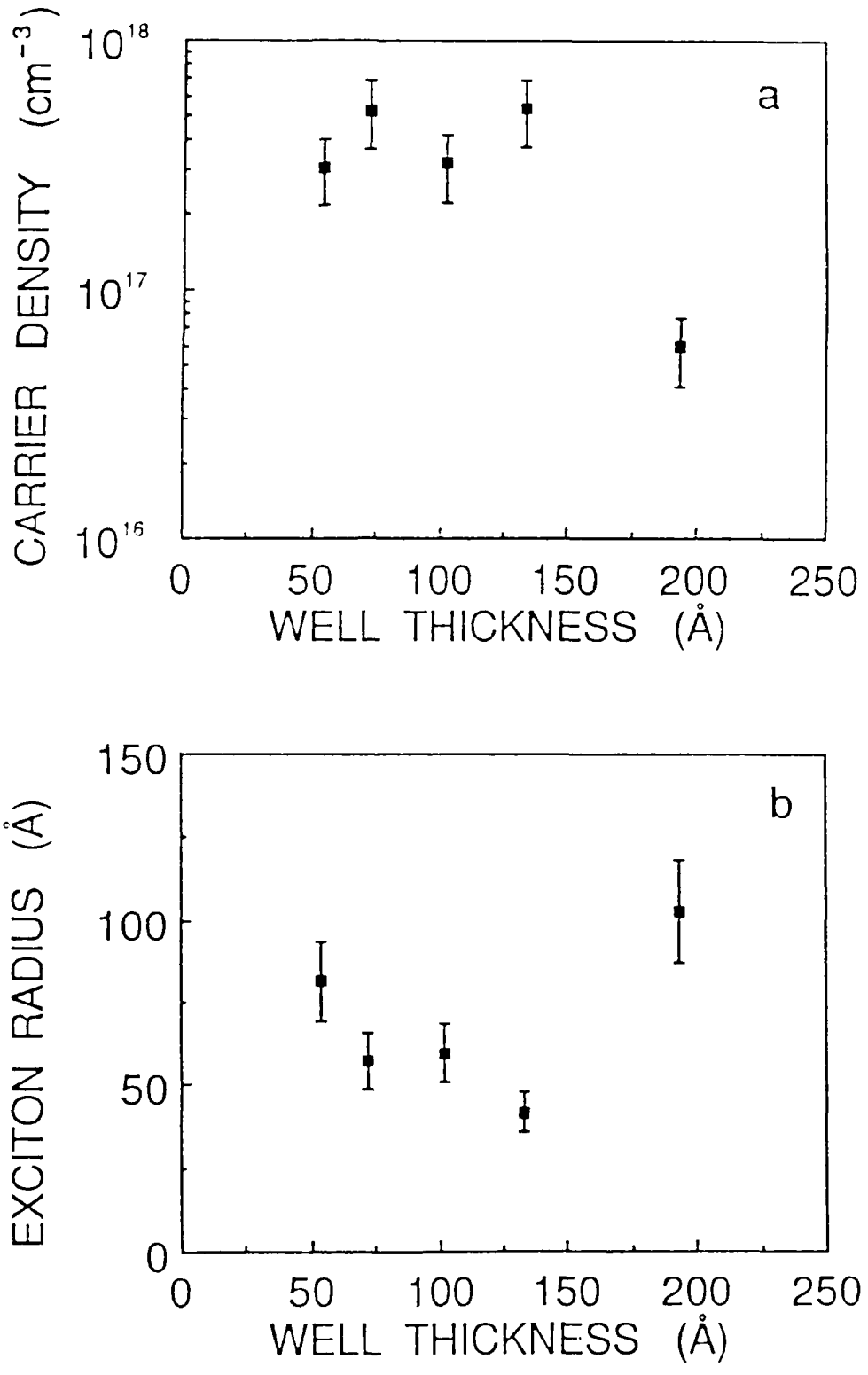
CARRIER DENSITY (cm^{-3})
10^{18}
10^{17}
10^{16}
a
0
50
100
150
200
250
WELL THICKNESS (Å)
EXCITON RADIUS (Å)
150
100
50
0
b
0
50
100
150
200
250
WELL THICKNESS (Å)

Fig.15

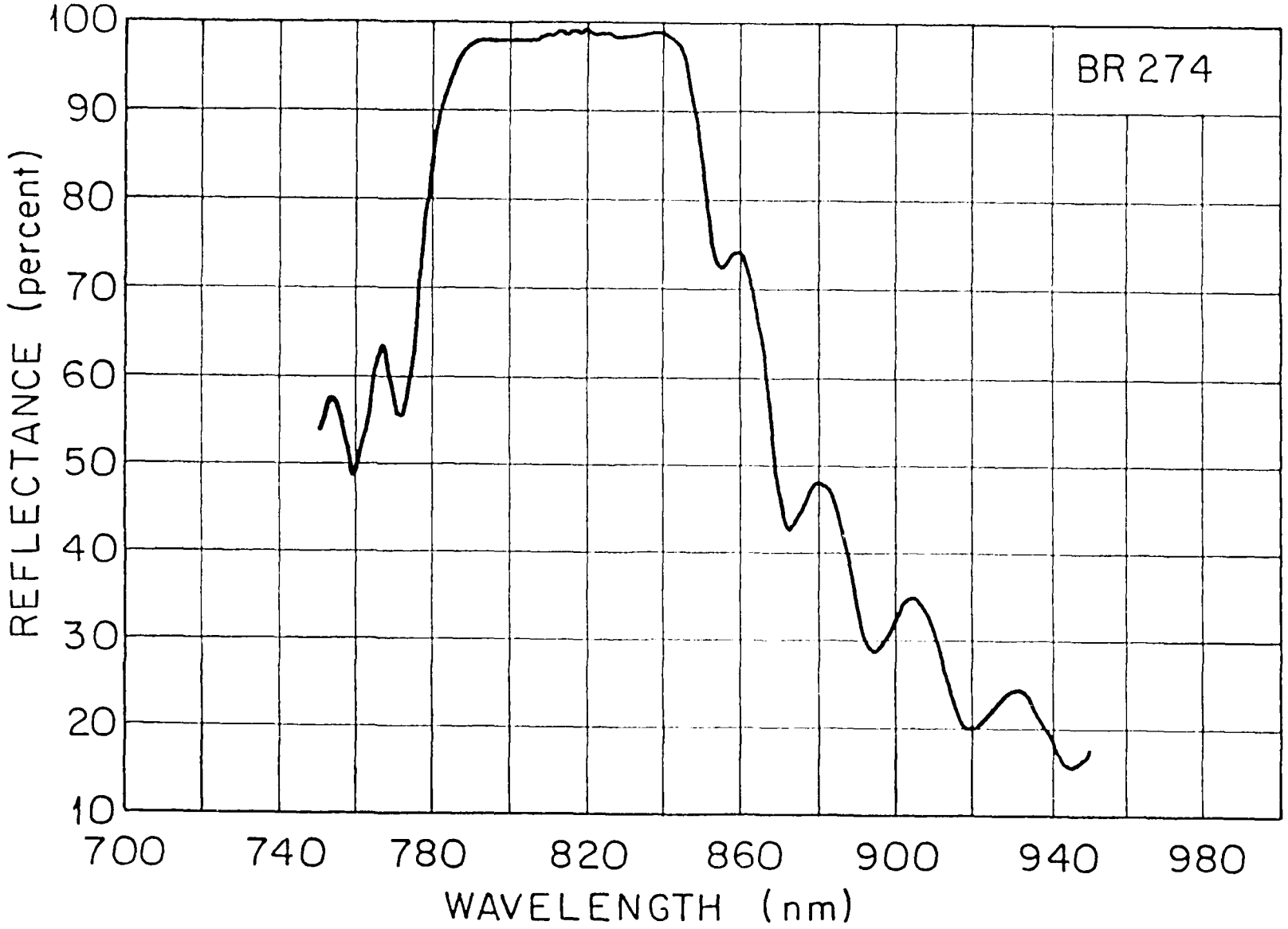
BR 274
REFLECTANCE (percent)
100
90
80
70
60
50
40
30
20
10
700
740
780
820
860
900
940
980
WAVELENGTH (nm)

Fig. 14

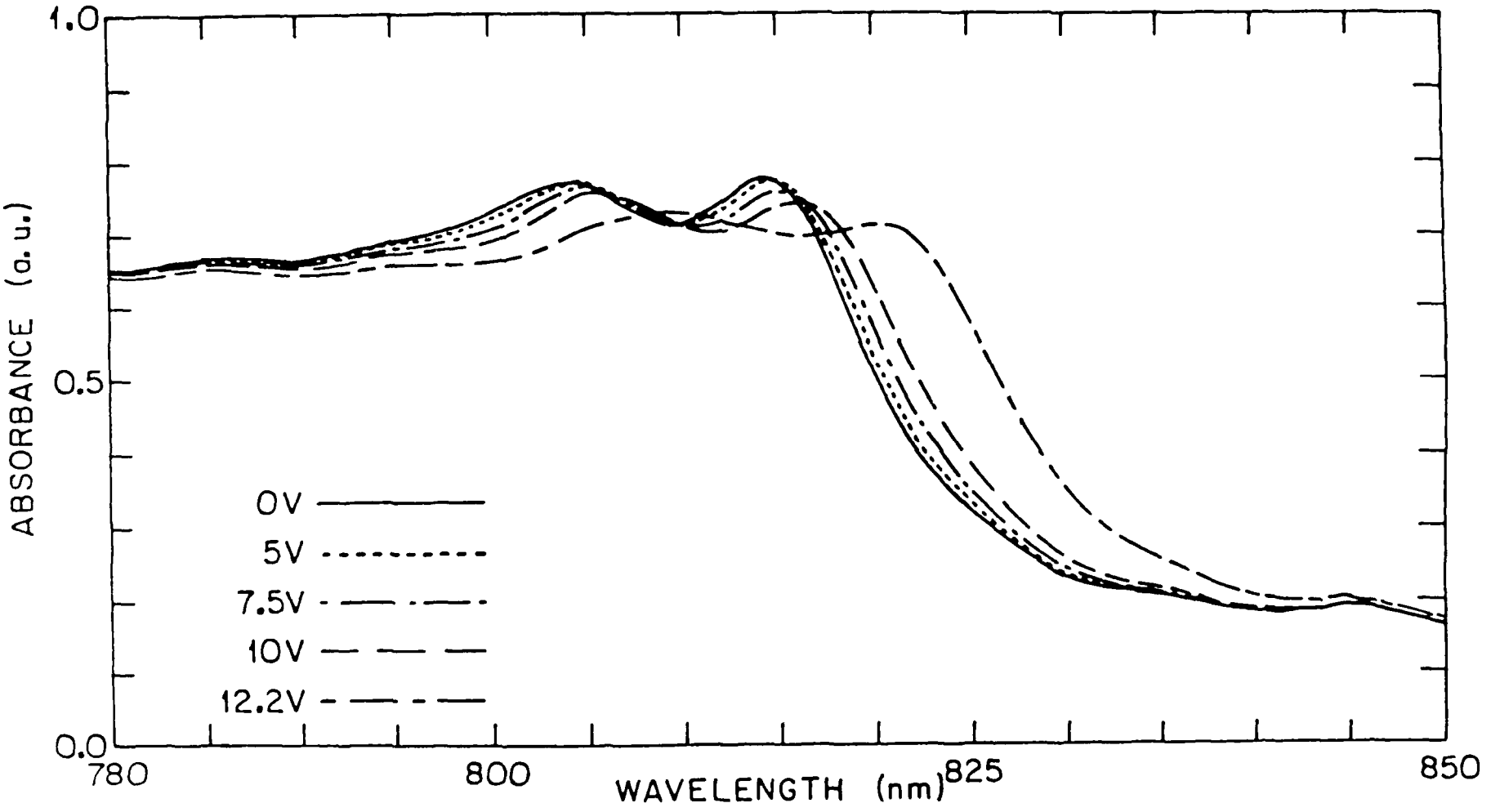
1.0
0.5
0.0
ABSORBANCE (a.u.)
0V
5V
7.5V
10V
12.2V
780
800
825
850
WAVELENGTH (nm)

Fig. 15

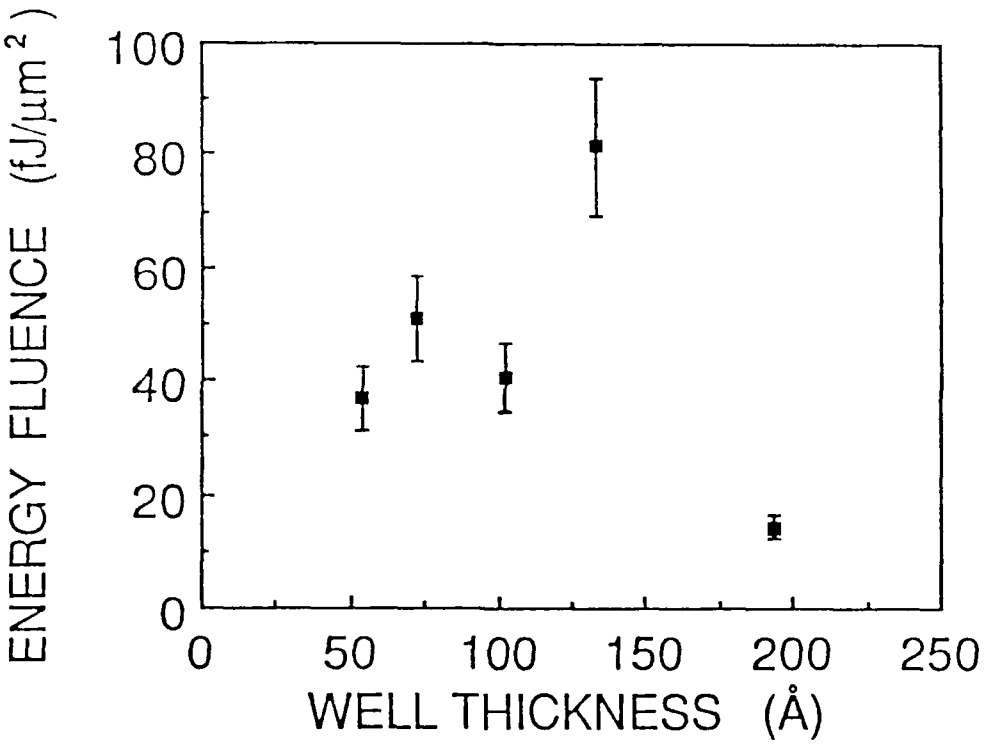
ENERGY FLUENCE (fJ/μm²)
100
80
60
40
20
0
0
50
100
150
200
250
WELL THICKNESS (Å)

Fig. 16

IV. Growth of high reflectivity Bragg reflectors and the electroabsorption of MQWs grown on GaP substrates.

To obviate the need for removing the GaAs substrate when implementing arrays of photonic switches, we have investigated the use of novel materials structures that rely upon the unique characteristics of MOCVD. The first of these is the DBR reflector. This is a multilayer stack of quarter wavelength layers that alternate in composition and, thus, refractive index. Through appropriate choice of materials composition it is possible to grow multilayer structure with exceedingly high reflectivity in a known spectral band that is also transparent to the reflected light. To match the wavelengths of light suitable for MQW application we have chosen to construct our reflectors from AlAs and $Al_{0.2}Ga_{0.8}As$ multilayer stacks. Fig. 1 shows a typical reflectivity spectrum from one of these samples. Several have been grown which show comparable results and device structures have been grown on top of them to verify that the surface morphology of the layers was maintained. These structures will allow us to fabricate reflective arrays utilizing NLFP or hybrid devices.

Transmissive devices presently require the removal of the GaAs substrate. We have recently demonstrated the growth of high quality MQW structures on transparent GaP substrates. We have measured the nonlinear absorption in these structures and found them to be exceedingly high (10000 W/cm2) ands unsuitable for NLFP devices. However we believe that these structures will be of great benefit in the fabrication of SEED and SEPT device structures. The electroabsorption properties of thes structure has been measured and is described in the following paper, published in Applied Physics Letters **51**,1582 (1987).

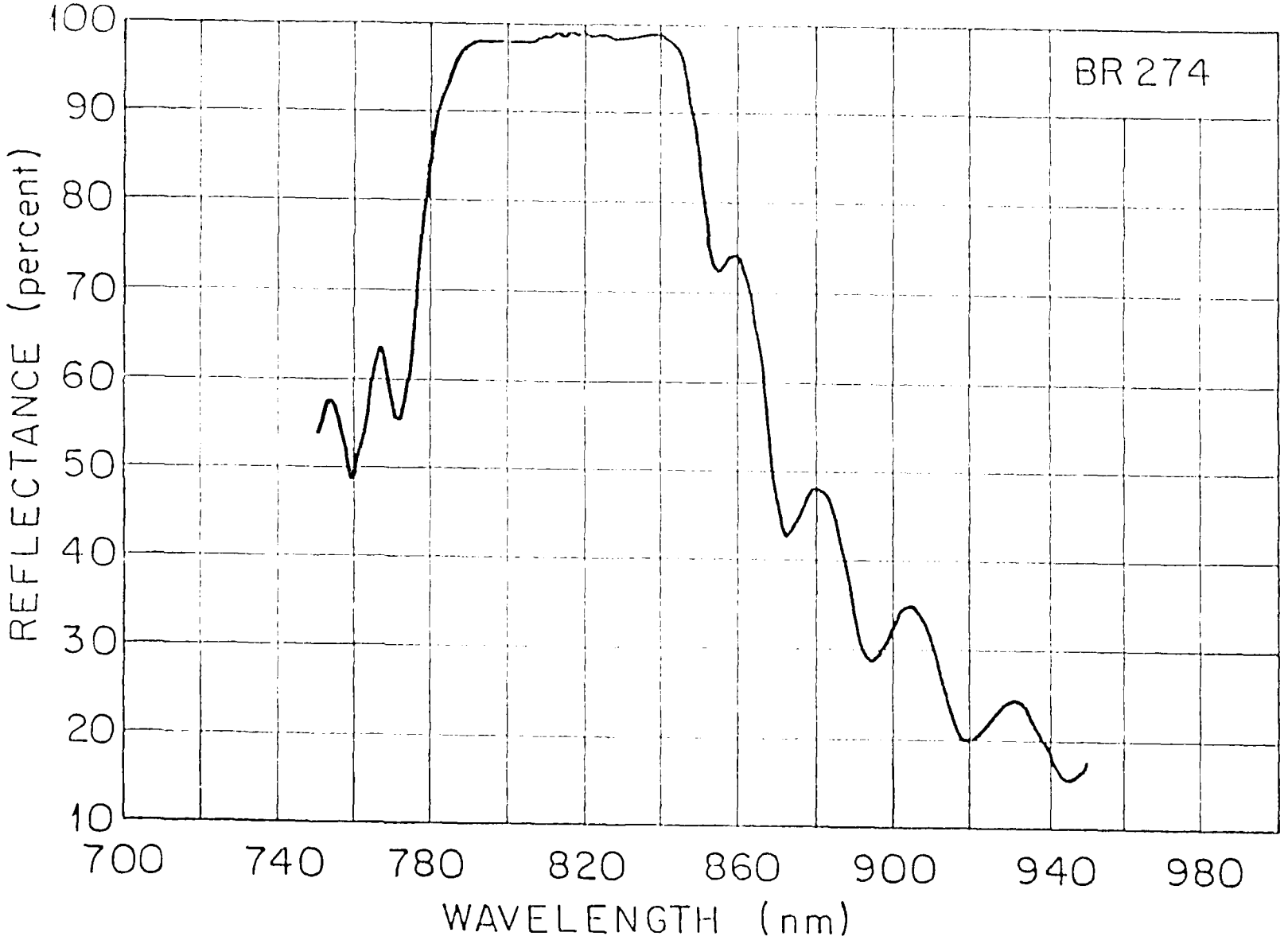
BR 274
REFLECTANCE (percent)
100
90
80
70
60
50
40
30
20
10
700
740
780
820
860
900
940
980
WAVELENGTH (nm)

Fig. 17

Electroabsorption in AlGaAs/GaAs multiple quantum well structures grown on a GaP transparent substrate

H. C. Lee,[a] K. M. Dzurko,[b] P. D. Dapkus, and E. Garmire
Department of Electrical Engineering and Center for Photonic Technology, University of Southern California, Los Angeles, California 90089-0483

(Received 22 July 1987; accepted for publication 3 September 1987)

The first measurements of electroabsorption in AlGaAs–GaAs multiple quantum wells grown on transparent GaP substrates are reported. High quality quantum well materials with sharp, well defined excitonic resonances are grown by employing a GaAsP intermediate layer between the quantum wells and the substrate. Good surface morphology and abrupt interfaces have been achieved with etch pit densities of 4×10^5 cm^{-2}. A 7.5-meV shift of the absorption edge to lower energies is observed for field strengths of 8×10^4 V/cm. These structures are well suited for photonic switch array fabrication.

One of the unique features of quantum wells which makes them attractive for observing optical nonlinearities is the existence of strong excitonic absorption at room temperature. Due to the electronic confinement properties of quantum wells, both the binding energy and oscillator strength of excitons are increased compared to those of the bulk GaAs. Narrow light- and light-hole exciton resonances are well resolved and observed at room temperature. These absorption resonances can be changed by photoexcitation or with an electric field. For an electric field applied perpendicular to the interfaces of quantum well layers, electrons and holes are pulled in opposite directions, while remaining confined by the potential barriers. As a consequence, the binding energy, electron and hole subband energies, and the optical oscillator strength are all modified by the electric field. This effect is known as the *quantum confined Stark effect* (QCSE).

Many applications have been demonstrated for the QCSE. High-speed modulators with multiple quantum wells (MQW's) in *p-i-n* structures have been reported.[1] Optical bistability and oscillation have been achieved in self-electro-optic effect devices (SEED's),[2] in which a coupled modulator and photodetector interact through external electronic feedback circuits. The crucial step for making these devices useful is to ensure that light will only experience the nonlinear region and will not be absorbed by the opaque GaAs substrate. The substrate is usually removed by selective etching, leaving a delicate 2–5 μm thick quantum well membrane. This step is difficult and not suitable for large area photonic switch fabrication.

In this letter, we describe the fabrication of high quality AlGaAs–GaAs multiple quantum well structures on transparent GaP substrates that obviate the need to remove the substrate and thus can potentially support the fabrication of large area arrays of photonic switches. We further demonstrate electroabsorption effects resulting from the QCSE in these materials that are suitable for the fabrication of photonic switches.

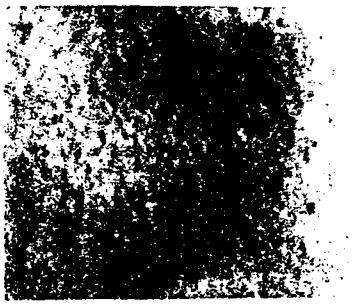

(a)

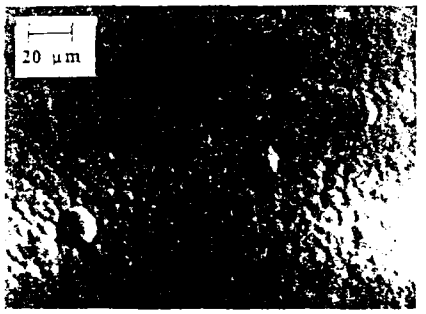

(b)

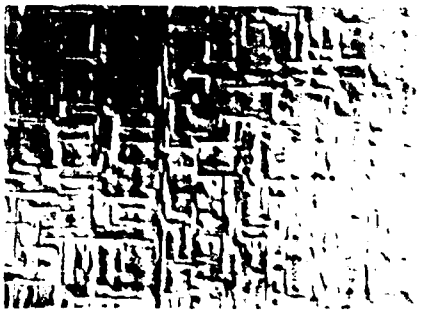

(c)

FIG. 1. Surface morphologies of (a) GaAs–Al$_{0.3}$Ga$_{0.7}$As MQW's grown on GaP with a GaAs$_{0.8}$P$_{0.2}$ buffer layer, (b) GaAs–Al$_{0.3}$Ga$_{0.7}$As MQW's grown on GaP with a GaAs$_{0.8}$P$_{0.2}$ buffer layer, $\Delta x = 2.5\%$ optimized layer, and (c) GaAs–Al$_{0.3}$Ga$_{0.7}$As MQW's grown on GaAs, $\Delta x = 2.5\%$ optimized buffer layer.

To accommodate the large lattice mismatch [illegible] between GaP and the AlGaAs/GaAs quantum wells, we grew an ungraded GaAs$_x$P$_{1-x}$ buffer layer with $x \approx 0.85$. The choice of this approach and detailed characterization of the structural properties of the resulting materials will be described in a separate publication currently in preparation. Quantum well structures with 100 periods, having well and barrier thickness of 50 and 150 Å, respectively, were grown on top of the GaAs$_x$P$_{1-x}$ buffer layer. The AlAs mole fraction in the barrier was 0.30. All samples were grown in a pressure balanced, atmospheric pressure metalorganic chemical vapor deposition (MOCVD) reactor. Trimethylgallium and trimethylaluminum were used for Ga and Al sources, respectively. Arsine and phosphine, purified through molecular sieves, were used as As and P sources, respectively. The GaAs$_x$P$_{1-x}$ was grown at 750 °C with a V/III ratio of 35 to a thickness of 4 μm. The quantum wells were grown at 700 °C. Lower growth temperatures for quantum wells were adopted to maintain sharp electron resonances.

Figure 1(b) shows the smooth surface morphology of GaAs$_x$P$_{1-x}$ grown on GaP. In this case, the GaAsP is [illegible] lattice mismatch is 2.3% [illegible] substrate [illegible]

[illegible] testing the back surface of the GaP substrate. Figure 2 shows a comparison of PL spectra of MQW's grown on a GaP substrate and on a GaAs substrate. Notice the slight shift of the spectrum on the long wavelength side for the sample grown on GaP. We believe this to be caused by either stress or interface roughness. However, both the PL peak

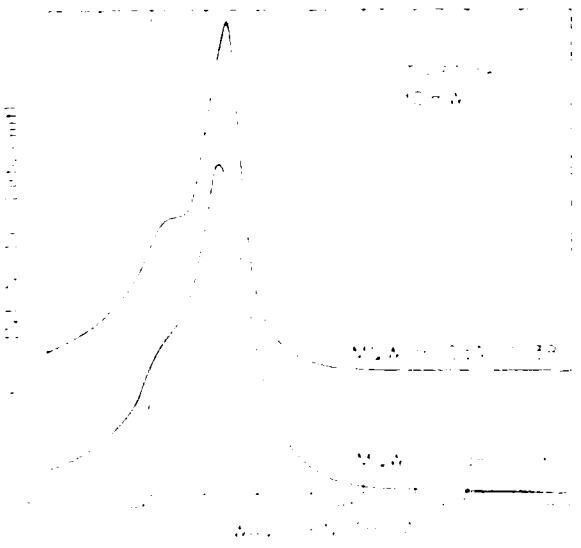

[illegible] spectra of MQW [illegible] GaP

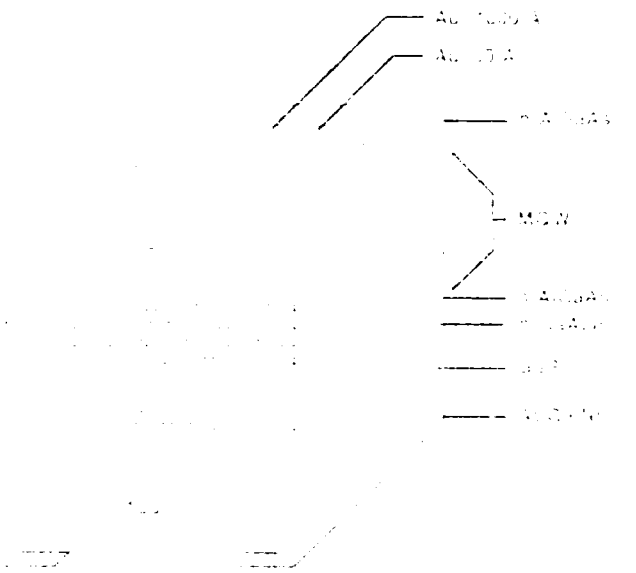

[illegible] a strong edge characteristic with a current concentration of [illegible] cm. The quantum well active region is a dense array. The sample was thinned to 150 μm, and a back side ohmic contact was deposited in an annular shape with AuGe/Ni/Au. A 50 Å Au Schottky barrier with 1000 Å Au contact fingers was evaporated on the top cladding layer. The transparency of the finger pattern is 90%. The edge of the top contact was removed by etching with KI:I$_2$:H$_2$O to minimize leakage current. The *I-V* characteristics of the device show a forward bias turn-on voltage of 0.8 V. The reverse bias leakage current is about 10 μA at −9 V for a 0.25-cm^2 device area. The reverse current increases strongly in the range −12 V to −13 V. The mechanism of this increase is not currently understood.

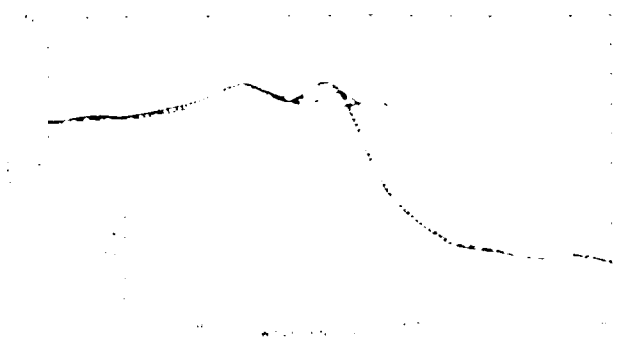

[illegible]

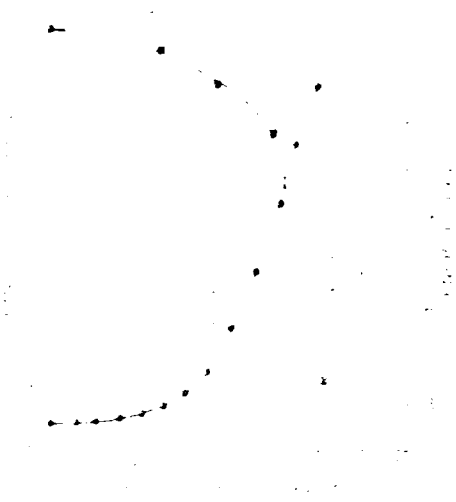

[illegible] wavelength of

[illegible] absorption spectra for reverse bias [illegible] 12 V. The shift of exciton resonance [illegible] the low-energy side [illegible] The shift to lower energy of the [illegible] and the decrease in the oscillator strength [illegible] are characteristic of the quantum-confined Stark effect observed in similar structures [illegible] Figure 5 shows the energy [illegible] which is about 7.5 [illegible] 12 V, the [illegible] electric field [illegible] reflects [illegible] the applied bias and the 2-V built-in voltage appearing across the active region. The figure also shows the absorbance at 823 nm increased by a factor of 2.5 with a bias change of 12 V. The absorbance was normalized [illegible] the maximum absorbance of the sample at zero field. The magnitude of the shifts observed in these samples is comparable in magnitude to that seen in materials grown on GaAs substrates. For use as active materials in bistable optoelectronic devices such as the SEED, a decrease in absorption with increasing voltage is necessary.[7] This is expected at higher voltages or at shorter wavelengths.

In conclusion, we have successfully grown high quality MQW's on a GaP transparent substrate with a single step GaAsP buffer layer. The electroabsorption observed in these samples is similar to that of samples grown on GaAs substrates,[7] suggesting that these structures will be an attractive alternative to the current practice of removing the GaAs substrate and should have significant impact on the fabrication of large area arrays of photonic switches in the future.

The authors gratefully acknowledge the Air Force Office of Scientific Research and the University of Southern California's Joint Services Electronics Program for partial support of this work.

[2] D. S. Chemla and D. A. B. Miller, J. Opt. Soc. Am. B [illegible] (1985).
[3] S. Schmitt-Rink, D. S. Chemla, and D. A. B. Miller, Phys. Rev. B [illegible] (1985).
[4] D. A. B. Miller, D. S. Chemla, T. C. Damen, A. C. Gossard, W. Wiegmann, T. H. Wood, and C. A. Burrus, Phys. Rev. Lett. 53, [illegible] (1984).
[5] T. H. Wood, C. A. Burrus, D. A. B. Miller, D. S. Chemla, T. C. Damen, A. C. Gossard, and W. Wiegmann, Appl. Phys. Lett. 44, [illegible].
[6] D. A. B. Miller, D. S. Chemla, T. C. Damen, T. H. Wood, C. A. Burrus, A. C. Gossard, and W. Wiegmann, IEEE J. Quantum Electron. QE-21, [illegible] (1985).
[7] H. C. Lee, A. Hariz, P. D. Dapkus, A. Kost, M. Kawase, and E. Garmire, Appl. Phys. Lett. 50, 1182 (1987).
[8] G. H. Olsen, M. S. Abrahams, C. J. Buiocchi, and T. J. Zamerowski, J. Appl. Phys. 46, 1643 (1975).
[9] D. S. Chemla, T. C. Damen, D. A. B. Miller, A. C. Gossard, and W. Wiegmann, Appl. Phys. Lett. 42, 864 (1983).

V. Implications of our research for optical computing applications.

The use of exciton resonance in MQW for an optical logic or switching devices means that a large nonlinear refractive index occurs because of a large amount of saturable absorption. We have found that at modest power levels there remains a relatively large amount of unsaturated absorption. It is the purpose of this section to consider the trade-off in performance between the size of the index change and the unsaturated absorption. We will design an nonlinear Fabry-Perot interferometer working on the exciton resonance, where the switching intensities are the lowest. Our design is based on the measured performance of MOCVD quantum wells. We will show that operation in reflection provides high contrast, low threshold, low loss operation. Conversely, operation in transmission is prohibitively lossy in the low threshold regime. This is a new result and has profound implications in design of future devices.

A. Material performance.

Figure 2a shows the change in measured absorption with varying input intensities as a function of wavelength within a MQW of well-width 100 A. Figure 2b shows the related change in refractive index at the same intensity levels as a fuction of wavelength. This curve was generated by using the Kramer's Kronig relation between the change in index of refraction $\Delta n(E)$ and the corresponding absorption change $\Delta\alpha(E')$:

$$\Delta n(E) = \left(\frac{ch}{2\pi^2}\right) P \int \frac{\Delta\alpha(E')dE'}{[E^2 - E'^2]} \qquad (1)$$

where E' denotes the photon energy at which the absorption change Δa is measured, E represents the photon energy at which the change in refractive index Δn is determined and P indicates that the integral is a Cauchy Principal Valve.

To use this relation, we found it necessary to convert a discrete set of measured points $\Delta\alpha(E'_i)$ into a continuous set by linear interpolation to avoid problems of convergence. We were then able to analytically integrate between the measured points. Using this method, the Kramers-Kronig relation becomes

$$\Delta n(E) = \sum_{i=0}^{n} \left(\frac{ch}{2\pi^2}\right) P \int_{E'_i}^{E_{i+1}} \frac{(m_i E + b_i)\, dE'}{E'^2 - E^2} \qquad (2)$$

where $m_i = \dfrac{\Delta\alpha_{i+1} - \Delta\alpha_i}{E'_{i+1} - E'_i}$ and $b_i = \Delta\alpha_i - m_i E'_i$

In this expression, E is the photon energy at which we calculate Δn, $\Delta\alpha_i$ is the ith absorption change measurement, made at photon energy E'_i, and m_i and b_i are the slope and horizontal intercept respectively of the line between $\Delta\alpha_i$ and $\Delta\alpha_{i+1}$.

The integral can be evaluated analytically to obtain:

$$\Delta n(E) = \left(\frac{ch}{2\pi^2}\right) \left\{ \frac{m_i}{2} \ln \left| \frac{E_{i+1}^2 - E^2}{E^2 - E_i^2} \right| + \frac{b_i}{2E} \ln \left| \frac{(E_{i+1} - E)(E_i + E)}{(E_{i+1}+E)(E_i - E)} \right| \right\}$$

The parameter which is of physical importance in device design for the nonlinear Fabry-Perot (NLFP) is the ratio of the index change to absorption change, as will be shown later. This ratio, calculated from experimental results, is shown in Figure 3.

B. Existence of Two Saturation Intensities

What is notable to the understanding of the use of the MQW in a NLFP is the fact that there are two satuaration intensities. This can be inferred from Figures 2 and 3. At incident power levels as low as 250 W/cm^2, it can be seen that the exciton saturates. That is, its absorption changes from 2.8×10^4 cm^{-1} to 2.1×10^4 cm^{-1}. This 30% change in absorption is not sufficient to cause any useful devices based on absorption alone. however, at this same power level of 250 W/cm^2, the induced refractive index change is as large as 0.038. This induced

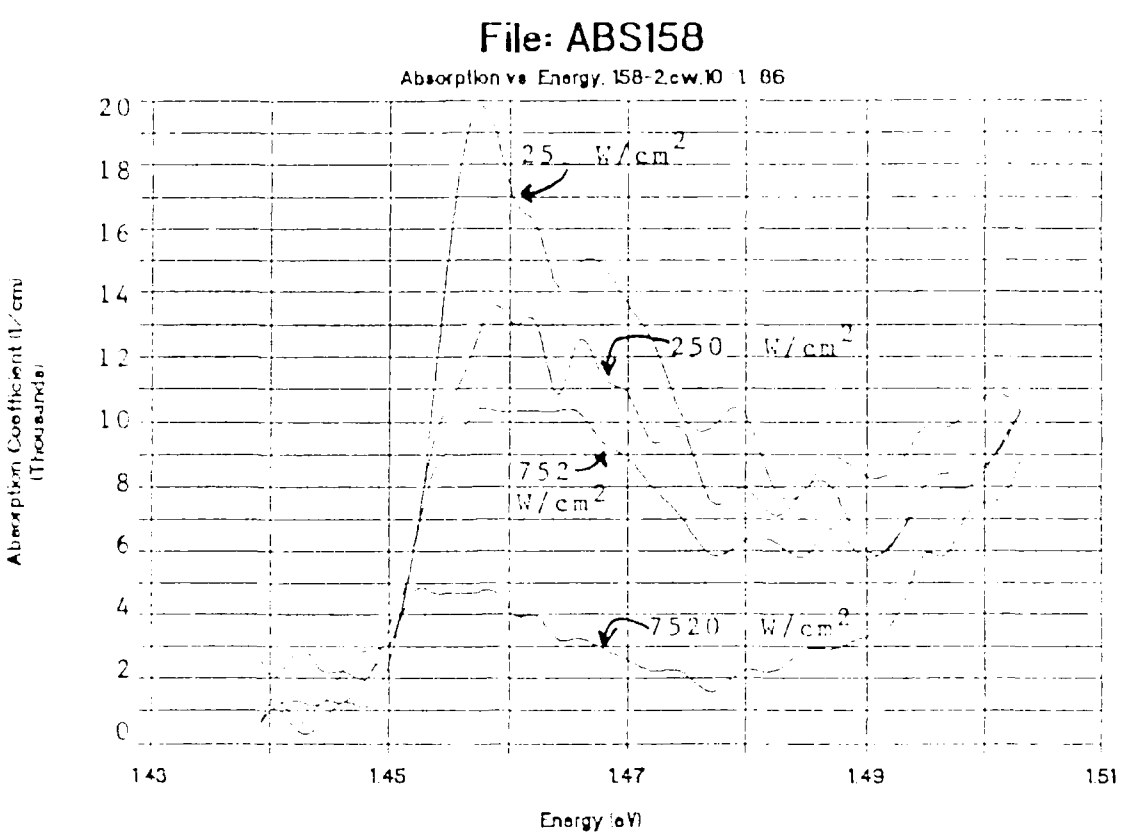

Figure 2a. Absorption as a function of energy for different levels of incident intensity for 100 A wells.

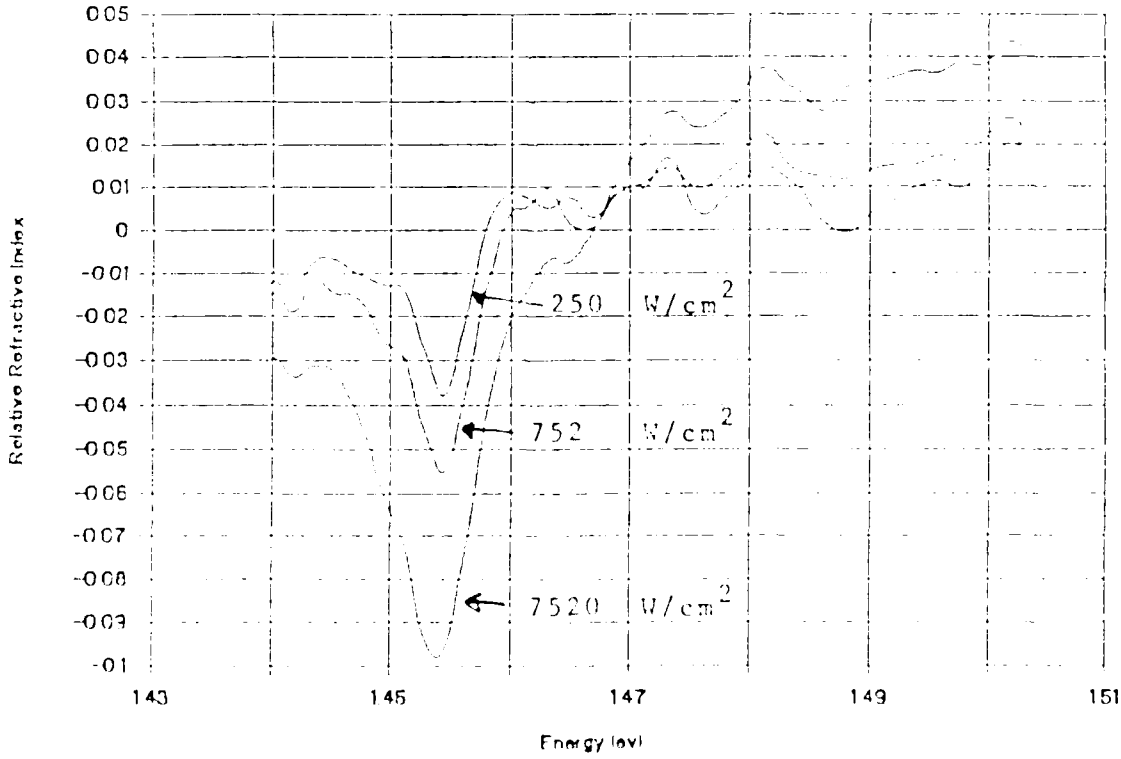

Figure 2b. Change in refractive index as a function of photon energy as a function of incident intensity, calculated from Kramers Kronig relations.

index change cannot make a switching device because of the large unsaturated absorption due to the band-to-band tails. However, we will show that it is not necessary to complete saturate the band-tails to induce switching. In fact, we predict switching with intensities of about 1000 W/cm^2 when operating right on the exciton resonance. By operating a NLFP in reflection, we find that excellent performance for optical computers can be attained.

First, however, we decided to investigate how to engineer a MQW with the minimum band tail absorption in the presence of saturated exciton resonance. This requires understanding the relative contributions to absorption from the two saturation mechanisms. In Figure 4 we show a careful study of the intensity dependence of the saturation energy, measured on the peak of the exciton resonance of a 100Å well sample. It can be seen that the absorption is composed of two compnents, that from the exciton resonance and that from the band tail. The absorption decreases from each mechanism, but with a different saturation intensity. It can also be seen that the contribution from each mechanism is initially comparable. At an intensity of 1000 W/cm^2 the exciton has almost completely bleached, while there has been very little reduction in the band edge absorption.

C. Dependence on Well Width

The question which must be answered for device applications is whether there is an optimum well size or an optimum wavelength at which the bandedge absorption is minimized in the presence of saturation exciton. For this reason we undertook a study of various well sizes and various excitation wavelengths. The results are summarized in Figure 5, which shows linear absorption measurements of these various wells and experimental data points which indicate the relative contribution of bandedge absorption and the exciton resonance.

The results of this extensive study were that for all well widths, the contributions to saturable absorption from exciton bleaching and band edge absorption are comparable. We also found, not surprisingly, that the ratio was largest directly on the exciton resonance.

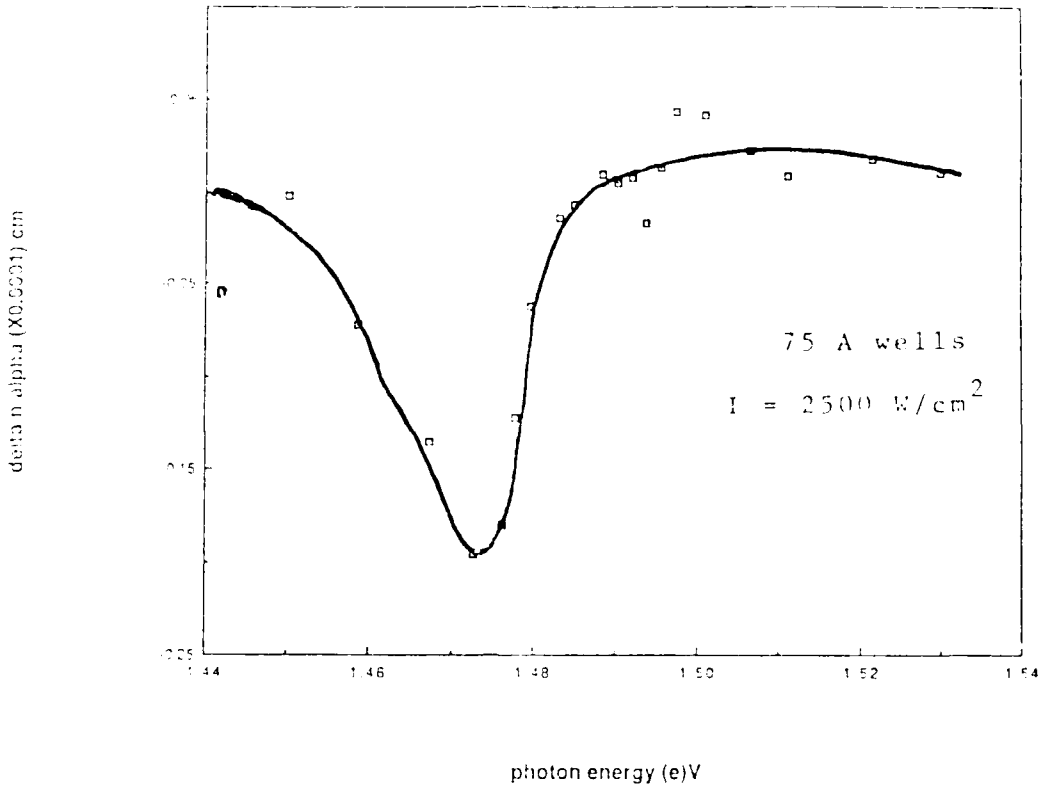

Figure 3. Ratio of induced refractive index to unsaturated absorption.

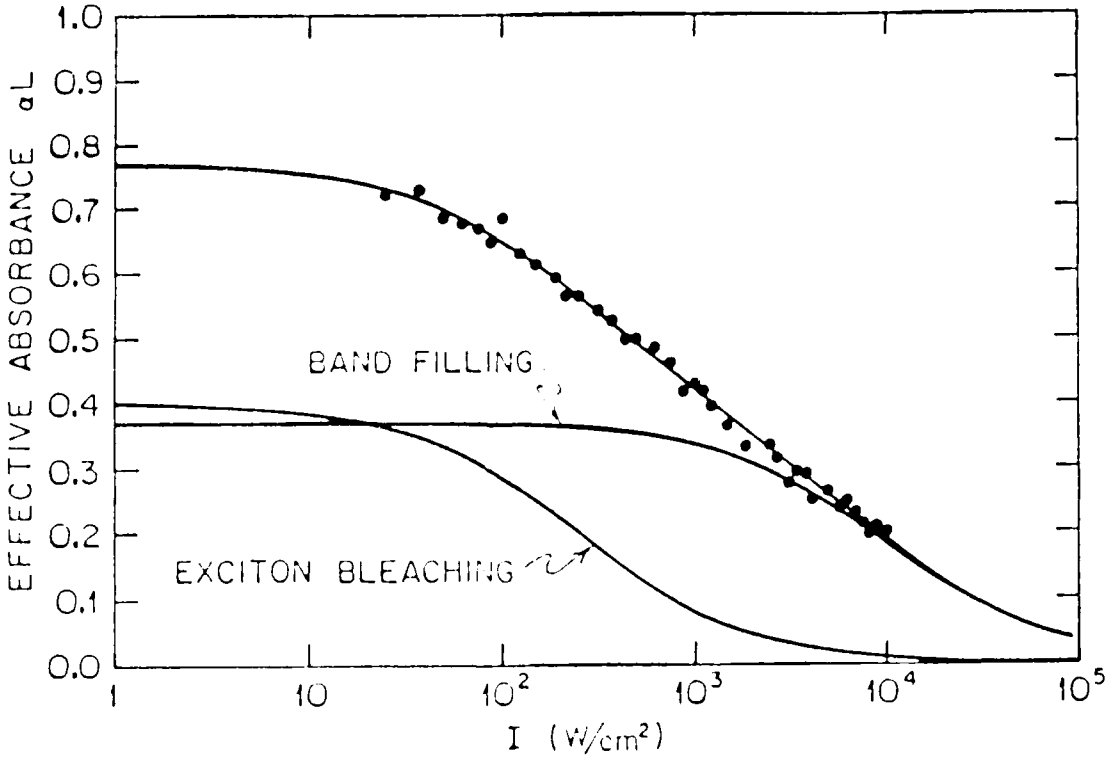

Figure 4. Absorption as a function of intensity, for the wavelength right on exciton line. Resulting two contributions from exciton bleaching and band filling are indicated.

The bottom line of this study is that at exciton bleaching intensities (~1000 W/cm^2) there remains roughly 50% unsaturated absorption. However, if the intensity is increased to 10,000 W/cm^2, even the band edge absorption can be bleached.

D. The Nonlinear Fabry-Perot Threshold

Because of the lower saturation intensity of the exciton feature, we were interested in exploring the operation of a NLFP in the presence of an overall unsaturated absorption. This loss will alter the performance of NLFP, which must be properly designed. It is the purpose of the following sections to show that the MQW's we have measured will provided a low threshold NLFP, operating in reflection with excellent characteristics for optical computing.

The transmission of a FP in the presence of loss can be written as [for example, see Craig Poole's Thesis, USC, 1984]

$$T = \frac{B}{1+F\sin^2\sigma} \tag{3}$$

where

$$F = \frac{4R_e}{[1-R_e]^2} \quad \text{and} \quad B = \frac{e^{-\alpha L}(1R_B)\,(1-R_F)}{(1-R_e)^2} \tag{4}$$

with

$$R_e = (R_F R_B)^{1/2} \exp(-\alpha L). \tag{5}$$

Note that neither F nor B depends on the order of the two reflectivities; that is whether, the large or small refractive index comes first. Note also that F does not depend on whether the two relfectivities are equal. It depends only on the effective reflectivity, R_e. In the absence of loss, B = 1 and the on-resonance trasmission is 100%. When loss is present, the on-resonance transmission drops. The introduction of loss also decreases the fraction F through the effective reflectivity,

The switching threshold in the presence of loss can be most easily seen by considering the graphical demonstration of the threshold for nonlinear switching (Figure 5), which plots the relation between the input and output light intensities,

$$I_{out}/I_{in} = T(\sigma), \tag{6}$$

where σ is half the round-trip phase change within the cavity. For arbitrary intensity-indued refractive index change, Δn, we write.

$$\Delta\sigma = \Delta n\ (I_{cav})dz. \tag{7}$$

The index change Δn is expressed in terms of the intensity inside the Fabry-Perot cavity, I_{cav}, which is, in general, a function of positon z within the FP, which we will measure from the output facet. The cavity intensity is related to the output intensity through,

$$I_{cav}(z) = C(z)I_{out}, \tag{8}$$

where

$$C(z) = \frac{e^{\alpha z} + R_B\, e^{-\alpha z}}{1-R_B}$$

The expression for C was fouund by adding forward and backward travelling waves inside the cavity and ignoring standing wave effects. When there is no loss, $C = (1 + R_B)/(1-4_B)$.

When the phase depends linearly on itensity and Δn - $n_2 I$, the round-trip phase change can be determined by a simple average, and

$$\sigma = n_2 \langle I_{cav}\rangle kL = DI_{out}, \tag{9}$$

where

$$D = n_2 \frac{e^{\alpha L}-1+R_B(1-e^{-\alpha L})}{\alpha(1-R_B)}k \quad = \quad n_2 \frac{(1-e^{-\alpha L})(R_B e^{-\alpha L}+1)e^{\alpha L}}{(1-R_B)\alpha}\ k.$$

When the propagation loss αL is much less than the reflection loss, $1-R_B$,

ABSORPTION OF MQW'S

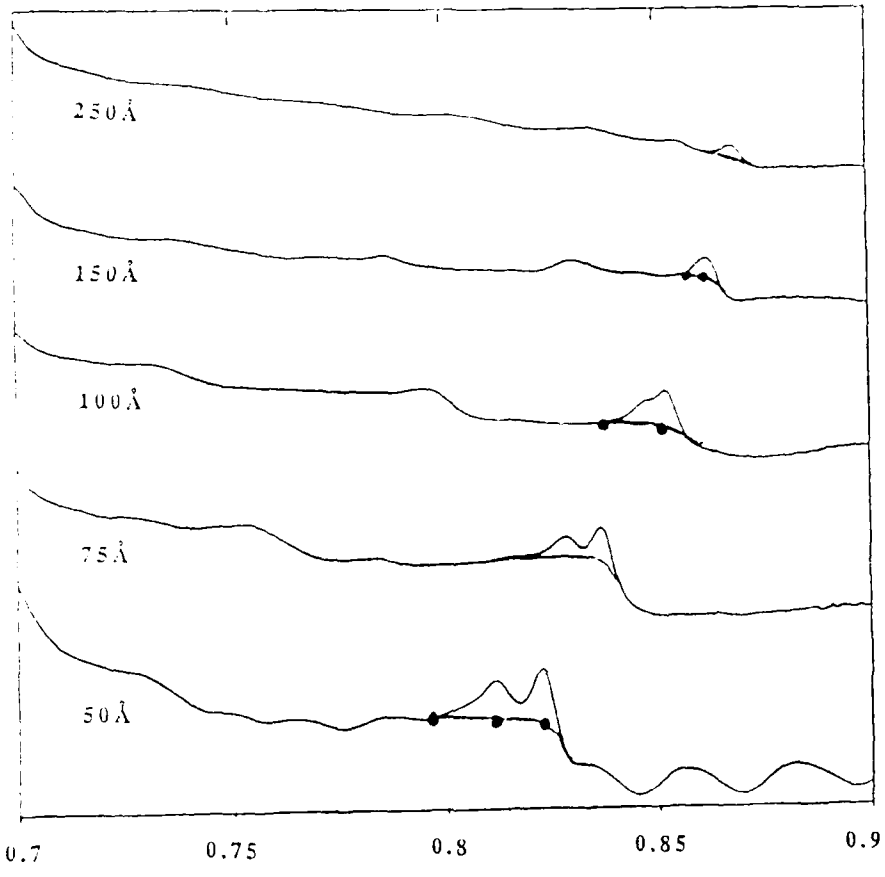

Figure 5. Linear absorption measured in MOCVD-grown multiple quantum wells. The dots represent the fraction of the absorption due to the background underneath the exciton feature, as measured by fitting to the saturable absorption.

$$\frac{\langle I_{cav} \rangle}{I_{out}} = \frac{(1+R_B)}{(1-R_B)} \qquad (10)$$

Figure 6 shows graphical plots of equation (6), which the right hand side is the transmission as a function of ø and the left hand side is a straight line of slope $1/DI_{in}$. Figure 5a shows four examples: a) at low intensity (large slope), in which there is only one intersection; b)at critical intensity, so that the slope of the straight line matches that of the FP transmission; c)at higher intensity, in which there are two stable intersections (the region of bistability); d) at highest critical intensity, which is the threshold for the switching from the low to high transmission state. This critical intensity is the threshold for optical bistability.

E. Requirements to achieve nonlinear switching.

There is a minimum critical intensity below which switching is impossible. This occurs at a particular round-trip phase bias, $ø_B$, as can be seen geometrically in Figure 5b. This bias ensures that the slope of the straight line intersects the transmission curve at the point of its maximum slope. From the figure it can be see that to have nonlinear switching, we must be able to change the round trip phase change $\Delta ø_c$ by an amount roughly equal to the half-width of the transmission resonance. When the finesse is reasonably large, this width is given by

$$\Delta ø_w = \frac{\pi}{2f} = \frac{1}{\sqrt{F}} \qquad (11)$$

where f is the fineese, defined by $f = \frac{2\pi}{F}$. This will occur at a zero-intensity bias phase for the FP of $ø_{Bo} \sim m\pi - \frac{\pi}{f}$.

The critical phase change can be re-expressed in terms of a critical average index change within the etalon, $ø_c = \langle \Delta n \rangle_c kL$. We write

$$\langle \Delta n \rangle_c = \frac{1}{kL}\sqrt{F}. \qquad (12)$$

Thus we minimize the required index change by maximizing

$$L\sqrt{F} = \frac{2\sqrt{R_e}\,L}{1 - R_e}$$

Clearly this is maximized by maximizing R_e. From equ. 4, it can be seen that R_e is maximized for maximum $R_F F_B$ and minimum loss. Defining $R_F = 1-T_F$ and $R_B = 1-T_B$, and expanding square roots and exponentials in Taylor series (assuming small loss),

$$1 - R_e = (T_B + T_F)/2 + \alpha L.$$

Defining a parameter μ such that $(T_B + T_F) = 2\mu\alpha L$, we may write

$$F_{max} = \frac{2}{\alpha(1+\mu)}.$$

Plugging the equation (14), we find a condition on $\Delta n/\alpha$ to observe switching:

$$\frac{(\Delta n)_{min}}{\alpha} = \frac{1}{2k}(1+\mu) = \frac{\lambda}{4\pi}(1+\mu). \qquad (13)$$

Equation (13) is a universal equation, valid in th elimit of small loss, indicating whether opical bistability is achievable in a given nonlinear medium. The importance of this equation is that we can then tell immediately from the data under what conditions the MWQ will be able to show optical bistabilility. For λ = 0.83μm, the data in figures 1 and 2 can be interpreted to show that the minimum cavity intensity for optical bistability in the limit that the material loss is comparable to the reflectivity loss ($\mu \sim 1$), is approximately 1000 W/cm^2. Under these condition, $\Delta n \sim -0.09$ and $\alpha \sim 6000$ cm^{-1}.

F. Minimization of Input Intensity to Observe Bistability

As long as the conditions of equation 13 are met by the nonlinear medium, bistability is possible. Let us consider how to design the cavity to minimize the input intensity into the NLFP to create switching. It will be most convenient to study the reflectivity of the FP:

$$R_{FP} = \frac{E + R\sin^2\Delta\sigma}{1 + R\sin^2\Delta\sigma} \qquad (14)$$

Here F is the same as before and

$$E = \frac{(R_F - R_e)^2}{R_F(1-R_e)^2}$$

It can be seen that when E = 0, the minimum reflectivity = 0. This will keep as much intensity inside the FP as possible and available for switching. This means that for the lowest input switching intensity we require.

$$R_F = R_e' \quad \text{or} \quad R_F = R_B \exp(-2\alpha L). \tag{15}$$

In order to calculate the required incident intensity, we notice from Figure 5 that the transmission at minimum switching threshold equals $\frac{3B}{4}$. This mean that

$$I_{out,\,m} = \frac{3B}{4} I_{in,m} \tag{16}$$

This expression allows us to relate the input intensity to the phase change within the cavity at switching through equation (9):

$$\sigma = D\frac{3BI_{in\,m}}{4}, \text{ which we set} = \frac{1}{\sqrt{F}} \tag{17}$$

This means $$I_{in,m} = \frac{4}{3B}\,\frac{1}{D\sqrt{F}}$$

or $$I_{in,\,m} = \frac{2\alpha}{3n_2k}\,\frac{(1-e)e^{\alpha L}}{\sqrt{R_e}(1-R_F)(e^{\alpha L}+R_B)(1-e^{-\alpha L})}$$

For any given loss, aL, we would like the back reflectivity to be as large as possible, since $(1-R_B\,e^{-2aL})$ is as small as possible for $R_B = 1$. In practice we are limited to a finite reflectivity R_B. We must choose the length L so that aL gives optimum performance. Here we assume R_B nd a are given and we calculate L. Looking at the variation in the above expression, it can be seen that the largest dependence is in the factor

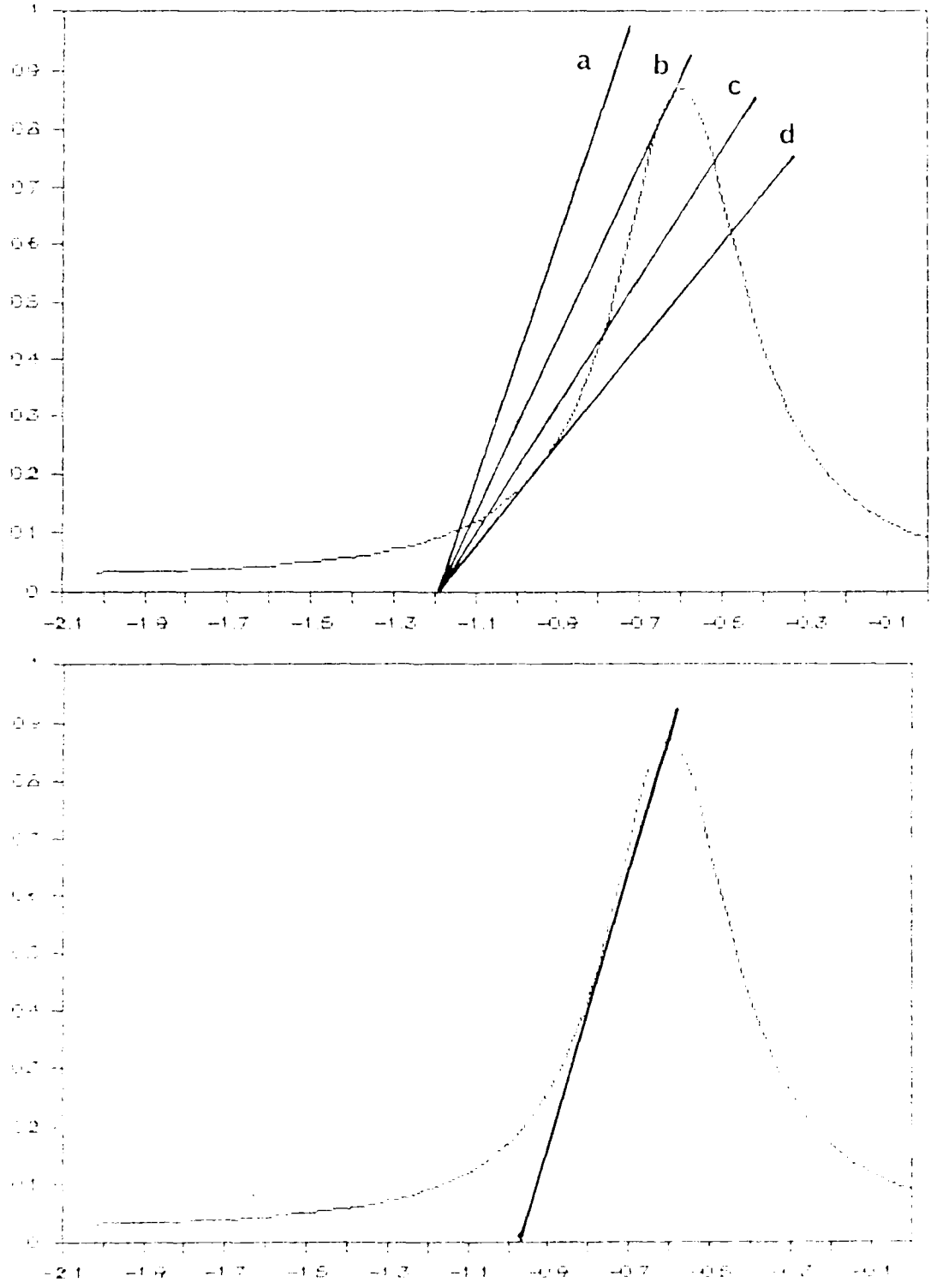

Figure 6. Graphical construction for the solution to a nonlinear Fabry-Perot. A) Solutions for arbitrary initial detuning; B) Solution for critical initial detuning.

$$X = \frac{(1-R_B e^{-2\alpha L})^2}{(1-e^{-\alpha L})}.$$

Assuming R_B is given, we set the differential of this expression equal to zero to obtain a condition for a minimum of incident intensity. The result is

$$e^{-\alpha L} = \frac{2}{3}\left(1 + \sqrt{(1-\frac{3}{4R})}\right).$$

In the limit of $R \rightarrow 1$, this given $e^{-\alpha L} \rightarrow 1$. Thus, write $R = 1-\mathcal{E}$. Then

$$A = \frac{2}{3}\left\{1+\sqrt{\frac{(1-4\mathcal{E})}{(1-\mathcal{E})}}\right\}$$

Expanding in a Taylor series, in the limit of small $\mathcal{E}$, $A = 1 - \frac{\mathcal{E}}{2}$. That is, $e^{-\alpha L} = 1 - \mathcal{E}/2$, or $2\alpha L = 1-R_B$. Thus, an optimum design has $R_B = 1-2\alpha L$, $R_F = R_B e^{-2\alpha L} = 1 - 4\alpha L$. This means that the loss in a round-trip through the medium equals the loss in the back mirror. The loss is the front mirror is two times the round-trip loss.

Inserting this cavity design into the required threshold intenity, Eq 3, under condition of low-loss,

$$I_{in,m} = (1-R_B)\frac{\alpha}{n_2}\frac{4\lambda}{3\pi}. \qquad (20)$$

The incident theshold is minimized by increasing the back reflectivity as much as possible. To compare this to the data on $\Delta n(I)$ which we determined experimentally, we write

$$I_{in,m} = \frac{\alpha I_m}{\Delta n}(1-R_B)\frac{4\lambda}{3\pi} \qquad (21)$$

where I_m is the intensity at which $\Delta n/\alpha$ is measured. Using the value $\Delta n = 0.2\mu m$, and the fact that $4\lambda/\pi = 1\ \mu m$, a reflectivity of $R_B = 96\%$ will give

$$I_{in,m} = 0.04\ I_m.$$

That is, if we assume Δn is proportional to I, the incident intensity can be as small as 4% of the intensity at which the value of $\Delta n/\alpha = 0.2\ \mu m$ was measure.

G Design of optimum NLFB based on MQW

We have found that the minimum $\Delta n/\alpha$ required to achieve bistability occurs for m (ratio of reflection loss to round-trip transmission loss) = 0. However, we have seen that the minimum incident intensity occurs for $\mu = 3$. Optimium peformance in a given system will require a trade-off between these two extremes of cavity design.

When $\mu = 3$ (the condition for minimum incident intensity) the reqauired $\Delta n/\alpha$ (from equ. 13) is $\Delta n/\alpha = \lambda/\pi = 0.26um$. However, from the data of Figure 1 and 2, the nonlinear index is not linear with intensity. This means that even high cavity intensities will not necessarily achieve the required n_2/α. To ensure bistability, it may be necessary to operate in the regime that $\mu<3$. This will lower the finesse and raise the required incident intensity, but will enssure sufficient cavity intensity that adequate $\Delta n/\alpha$ can be achieved.

A good compromise is $\mu = 1$. This means we require $\Delta n/\alpha = \lambda/2\pi = 0.13\ \mu m$, which our data tells us is achievable. In this case we cooshe $T_B - T_F = 2\alpha L$, $R_F = R_e$ and specify R_B. This gives the cavity design shown in the Table. The incident threshold intensity can be calculated from eq. 19; or in the low-loss limit,

$$I_{in,m} = \frac{2\alpha}{3\Delta n}(I_m)\frac{\lambda}{4\pi}\ \frac{(T_B + 2\alpha L)^2}{\alpha L} \qquad (22)$$

Here we express the incident threshold intensity as a fraction of the intensity I_m used to measure $\alpha/\Delta n$.

For the $\mu = 1$ case considered here, we require $\frac{\Delta n}{\alpha} = \frac{\lambda}{2E}$. Inserting this into the above equation,

$$I_{in,\,m} = (I_c)\frac{(T_B + 2\alpha L)^2}{3\alpha L}, \qquad (23)$$

where I_c is the intensity required to attain $\Delta n/a = \lambda/2\pi = 0.13$. Plugging in numbers from the experimental data for the 75Å sample, and extrapolating between measurements at 400 and 2500 W/cm2, we determine that I_c = 1000 W/cm2, and we predict a threshold of between 100 and 200 W/cm^2.

Table I. Modelling for a NLFP

Case I (High Reflectivity Back Mirror)

$R_B = 0.98$, $\alpha L = 0.05$, $R_F = 0.05$, $R_F = 9.92$ $I_{in,m} = 0.15I$
$I_{in,m}$ = 100 W/cm^2, P_m = = 0.6mW. L = 0.08 μm = 800 Å.

Case II (Lower Reflectivity Back Mirror)

$R_B = 0.95$, $\alpha L = 0.1$, $R_F = 0.85$. I = 01I.
$I_{in,\,m}$ = 200 W/cm^2, P_M = 0.12mW. L = 0.167 um = 1670Å.

For a minimum spot size of 25 μm X 25 μm (in the absence of diffusion), the predicted switching intensity gives a switching power of 0.6mW per pixel, or two orders of magnitude lower than has previously been observed.

The favorable numbers obtained in this optimization suggest that we operate in this regime, where $\Delta n/a$ has its largest value. This requires the use of very thin cavities, determined from the small values of αL. For our estimate of α = 0.6 μm^{-1} at switching threshold, this means MQW material thickness of only 1000 Å. This length indicated here is that of the quantum wells only, each typically 75 Å thick, so that the optimized NLFP will contain only ten to twenty quantum wells. When the thickness of 100 Å cladding per quantum well is included, the overall thickness of NLFP will be on the order of 2000 Å to 4000 Å. Why bistability has not been seen previously at such low power levels as we predict here is due to the fact that thin enough samples have not been investigated. Growth on reflective or transparent substrates will allow such thin samples to be prepared easily.

H. Performance of NLFP

We will show that when optimized for switching with low threshold, the performance of the NLFP in reflection is much than in transmission. This is because of the existence of substantial losss in the transmission device. We will also show that the NLFP in reflection has an output of almost 100% and an off-state of zero. This is ideal for an optical computer.

The transmissive FP is characterized by its maximum and minimum transmission (at $\phi = 0$ and $\phi = 90^{\circ}$):

$$T_{max} = B \qquad T_{min} = \frac{B}{(1+F)}.$$

When there is no loss, B = 1 and $T_{max} = 1$. Otherwise, when $R_F = R_e$,

$$B = \frac{(1-R_B)\, e^{-\alpha L}}{1-R_e} \tag{24}$$

For small loss, and under the conditions that $\mu = 1$, we may write

$$B = \frac{T_B}{2\alpha L}. \tag{25}$$

This means that, for our two cases considered above, B has values of 0.2 and 0.25; at least 3/4 of the light will be lost to absorption when the FP has its maximum transmission. Any attempt to reduce the loss will increase the threshold unacceptably. Clearly the MQW NLFP in transmission is not a useful device.

However, consider the NLFP in reflection. In this case the relevant requations are:

$$R_{min} = E, \quad R_{max} = \frac{E+F}{1+F} \tag{26}$$

In our previous analysis we have chosen $R_F = R_e$ so that E = 0. This means that the minimum reflectivity is zero. The maximum reflectivity is

$$R_{max} = \frac{F}{(1+F)} = \frac{1}{[1+1/F]}.$$

As before, when the loss is small, and under the optimum condiition, $1-R_e = 2\alpha L$:

$$\frac{1}{F} = \frac{[1-R_{eff}]^2}{4R_{eff}} \approx (\alpha L)^2.$$

Thus $$R_{max} = \frac{1}{[1+(\alpha L)^2]} \approx 1.$$

The result of this analysis is that a NLFP used in reflection has a maximum reflectivity of almost one and a minimum reflectivity of zero. This is therefore much more practical than an NLFP used in transmission.

I. Conclusions

It can be seen that the experimental data from our study of the MQW can be used to design a NLFP with a threshold for switching of only 0.6 mW threshold by designing a thin structure only ten quantum well thick and operating on the peak of n/α. Under these conditions the reflective NLFP is much more useful for optical computing than transmissive NLFP's. We can achieve large contrast ratio with high output in the high state as well as low threshold. If three-port devices are required using a relfective device, these may include two polarizations, or the use of light incident at small angels. What is required in the next phase of this study is a more complete systems study of the use of NLFP's in reflection.

VI. Summary and Recommendations

The work described in this report represents the first systematic investigation of the nonlinear optical properties of MQW structures. The conclusions of section V show that the structures investigated here will be useful primarily as reflective modulators with extremely high contrast ratio. As transmissive medium the MQW's are most easily used as the active element in SEED or other hybrid optoelectronic devices.

The study we have completed shows also that MOCVD, under the apprpriate growth conditions, is a most suitable growth process for the fabrication of nonlinear MQW structures. Low saturation intensities and large excitonic

absorption is attained when the materials are grown in the appropriate temperature range. Furthermore the technique has been used to grown two structure that allow the extension of MQW structures to large array structures by obviating the need to remove the substrate. For reflective NLFP or hybrid devices, we have demonstrated that high reflectivity Bragg reflectors can be grown and incorporated into optical structures. We have also demonstrated the growth of high optical quality MQW structures on GaP substrates that can be incorprated into hybrid optoelectronic devices.

The results of this program lead to three main recommendations for further study:

(1) Exploration of the use of GaP substrates in hybrid optoelectronic devices such as the SEEd and SEPT should be undertaken with the goal of fabricating large arrays of switches. This study should include fundamental study of the materials issues in this heteroepitaxial system, detailed study of the effects of strain on the relevant optical properties, and device studies to optimize a hybrid structure.

(2) *Exploration of the use of reflective* NLFP, *in optical computing* systems and the fabrication of arrays of such devices. In this regard we expect that other structure than the simple MQW deserves exploration to achieve similar Dn/a at lower excitation.

(3) A fundamental study of the band edge absorption in MQW structures including a detailed study of the continuum background absorption is required to determine if the observations of this work and others in the literature are general and fundamental. This study may allow the fabrication of high performance transmissive NLFP's for selected applications.

END

DATE

FILMED

5-88

DTIC